NASA/CR—2005-213643/PART2

Characterization of Ice for Return-to-Flight of the Space Shuttle

Part 2—Soft Ice

Erland M. Schulson and Daniel Iliescu
Dartmouth College, Hanover, New Hampshire

October 2005

The NASA STI Program Office . . . in Profile

Since its founding, NASA has been dedicated to the advancement of aeronautics and space science. The NASA Scientific and Technical Information (STI) Program Office plays a key part in helping NASA maintain this important role.

The NASA STI Program Office is operated by Langley Research Center, the Lead Center for NASA's scientific and technical information. The NASA STI Program Office provides access to the NASA STI Database, the largest collection of aeronautical and space science STI in the world. The Program Office is also NASA's institutional mechanism for disseminating the results of its research and development activities. These results are published by NASA in the NASA STI Report Series, which includes the following report types:

- TECHNICAL PUBLICATION. Reports of completed research or a major significant phase of research that present the results of NASA programs and include extensive data or theoretical analysis. Includes compilations of significant scientific and technical data and information deemed to be of continuing reference value. NASA's counterpart of peer-reviewed formal professional papers but has less stringent limitations on manuscript length and extent of graphic presentations.

- TECHNICAL MEMORANDUM. Scientific and technical findings that are preliminary or of specialized interest, e.g., quick release reports, working papers, and bibliographies that contain minimal annotation. Does not contain extensive analysis.

- CONTRACTOR REPORT. Scientific and technical findings by NASA-sponsored contractors and grantees.

- CONFERENCE PUBLICATION. Collected papers from scientific and technical conferences, symposia, seminars, or other meetings sponsored or cosponsored by NASA.

- SPECIAL PUBLICATION. Scientific, technical, or historical information from NASA programs, projects, and missions, often concerned with subjects having substantial public interest.

- TECHNICAL TRANSLATION. English-language translations of foreign scientific and technical material pertinent to NASA's mission.

Specialized services that complement the STI Program Office's diverse offerings include creating custom thesauri, building customized databases, organizing and publishing research results . . . even providing videos.

For more information about the NASA STI Program Office, see the following:

- Access the NASA STI Program Home Page at ***http://www.sti.nasa.gov***

- E-mail your question via the Internet to help@sti.nasa.gov

- Fax your question to the NASA Access Help Desk at 301–621–0134

- Telephone the NASA Access Help Desk at 301–621–0390

- Write to:
  NASA Access Help Desk
  NASA Center for AeroSpace Information
  7121 Standard Drive
  Hanover, MD 21076

NASA/CR—2005-213643/PART2

Characterization of Ice for Return-to-Flight of the Space Shuttle
Part 2—Soft Ice

Erland M. Schulson and Daniel Iliescu
Dartmouth College, Hanover, New Hampshire

Prepared under Cooperative Agreement NNC05VA04P

National Aeronautics and
Space Administration

Glenn Research Center

October 2005

Available from

NASA Center for Aerospace Information
7121 Standard Drive
Hanover, MD 21076

National Technical Information Service
5285 Port Royal Road
Springfield, VA 22100

Available electronically at http://gltrs.grc.nasa.gov

Contents

10. Figures

CHARACTERIZATION OF ICE FOR RETURN-TO-FLIGHT OF THE SPACE SHUTTLE PART 1—HARD ICE

Erland M. Schulson, Daniel Iliescu, and Andrew Fortt
Dartmouth College
Hanover, New Hampshire 03755

ABSTRACT

In support of characterizing ice debris for return-to-flight (RTF) of NASA's space shuttle, we have determined the microstructure, density and compressive strength (at -10 °C at ~0.3 s^{-1}) of porous or "soft" ice that was produced from both atmospheric water and consolidated snow. The study showed that the atmospheric material was generally composed of a mixture of very fine (0.1-0.3 mm) and coarser (5-10 mm) grains, plus air bubbles distributed preferentially within the more finely-grained part of the microstructure. The snow ice was composed of even finer grains (~0.05 mm) and contained more pores. Correspondingly, the snow ice was of lower density than the atmospheric ice and both materials were significantly less dense than hard ice. The atmospheric ice was stronger (~3.8 MPa) than the snow ice (~1.9 MPa), but weaker by a factor of 2-5 than pore-free hard ice [Schulson et al. 2005] deformed under the same conditions. Values are given for Young's modulus, compressive strength and Poisson's ratio that can be used for modeling soft ice from the external tank (ET).

1. INTRODUCTION

In this report we describe the second part of a study on the characterization of ice, for use in NASA's program on return-to-flight of the space shuttle. Part-I [Schulson et al. 2005] addressed "hard" ice, which is defined as fully-dense, optically transparent material. That report presented measurements we made of the brittle compressive strength versus microstructure (polycrystals and single crystals), with different amounts of prior damage (D = 0 and D ~ 0.3). We varied strain rate (0.01 s^{-1} to 1.6 s^{-1}), temperature (-10 °C and -38 °C > T > -71 °C), and length-to-diameter ratio of cylindrical specimens (L/D = 2.2 and 0.25). Here, we focus on "soft" ice, which is defined as porous and thus opaque material. We describe its microstructure and report its density and brittle compressive strength from measurements at -10 °C. Also, we discuss the tensile strength and the elastic properties of porous ice, from a review of the literature.

Soft ice, as it pertains to the space shuttle, encompasses a relatively broad range of material that forms either directly from water in the atmosphere or after condensation. At one extreme is the acreage of frost that forms over much of the exterior surface of the foam-covered external fuel tank (ET) whose inner surface is at either -183 °C (in contact with liquid oxygen) or -253 °C (liquid hydrogen). At the other extreme is the higher-density material that forms directly on cold metal, such as the bellows of the 17-inch diameter liquid oxygen (LOX) feedline that runs 70 feet down the lower half of the 153.8 foot tank. Pieces of ice as small as ~10 grams falling from the external tank and striking a sensitive part of the shuttle's wing at a relative velocity of ~500 miles per hour may create enough damage to seriously affect the integrity of the structure, judging from the effect of a small piece of foam of similar mass [Schwartz 2005].

Our aim is not to assess potential damage to the orbiter. Instead, it is to provide basic information on the strength of ice that can be used as input to modeling. We describe our findings in this report. The report and raw test sample data files have been placed on the Orbiter TPS Impact Testing Data Archive website at NASA Johnson Space Center, JSC. The link for the website is http://hitf.jsc.nasa.gov/hitfpub/archive/home.cfm. The data can be found in series 50 "Characterization of ice used for impact testing". Requests for access to the site should be submitted via email to: james.l.hyde1@jsc.nasa.gov.

2. THE ICE

Four separate programs supplied the ice represented in this report. The purpose of the first program was to manufacture and supply low-density ice for ballistic impact testing. This ice was supplied by Greg Sherrill at Aerotek-JSC. Most of the characterization work done in this report was in support of "Project Iceball" run by Darrell Holloway from USA-KSC. The project was designed to support launch day decisions based on ice/frost formations that occur under cryo loading. It was hoped to gain some characterization information on what type of ice formed on actual ET panels and relate this to the corresponding properties of the ice and subsequently to the potential damage caused by impact. The ice was made and sent to us by Paul Macaluso from Lockheed Martin – Michoud Assembly Facility (LM-MAF). Foamed panels were created according to standard ET configurations. The panels were tested in a humidity chamber at various ambient temperatures and relative humidities to simulate the range of icing environments at the launch site in Florida. The panels were chilled using a cryo backface. Formations of ice were removed from the panels and shipped to Dartmouth for characterization. Ice was supplied from both Phase I and II of LM-MAF Test Plan 809-9567. For the third program, ice was supplied by Ricardo Machin at NASA-JSC. This ice was supporting the efforts investigating aerodynamic breakup of the ice that might be released from the LOX feedline bellows. The question to be answered was: if the ice were released from the bellows, would it break into small enough pieces that it would not be of an impact concern during ascent? This was studied by injecting an 8 in. arc of ice into a Mach 3.5 flow field and observing its behavior. Characterization of the ice was performed to provide estimated strength data for modeling the wind tunnel experiment. Additionally, we desired to know the microstructure for comparison to other ices used in the RTF program. Finally, we also made material in the Ice Research Laboratory (IRL) at Dartmouth by compacting snow. This was done to provide another possible source and manufacturing method for low-density ice. Low-density ice was dropped from the RTF program and this effort was cancelled.

To distinguish one batch of ice from another, we continued the enumeration used in of Part-I. There we ended with Ice-14, the 14th and last shipment we examined for that study. Here we begin with Ice-15 and end with Ice-25. Table 1 sets this out. Included in the list is the snow ice we prepared in the Ice Research Laboratory (IRL). Excluded are Ice-23 and Ice 24: both shipments contained hard ice only, the former in the form of 12 solid cylinders (1.25 in. dia. x 3 in.) from NASA-Glenn and the latter in the form of discs (~0.8 in dia.) from Case Western Reserve University. Ice-23 was in storage in the IRL at the time of writing. Ice-24 was characterized and described in a separate report dealing with the high strain rate behavior of ice [Shazly et al. 2005]. The size, shape and number of specimens varied from lot to lot. Ice-15 (from LM-MAF) consisted essentially of 10 irregularly-shaped specimens that weighed < 2.6 grams each. Ice-16 (Aerotek-JSC) contained 8 prismatic-shaped specimens ~1.5 in. x 1 in. x 0.25 in. Ice-17 from Aerotek-JSC contained 7 prisms, but larger, ~2 in. x 2 in. x 3.5 in. In this

case, a significant amount of material had broken off from the specimens, resulting in less than regular shapes. Ice-18 (Aerotek-JSC) consisted of 13 solid cylinders, ~0.8 in. dia. x 1.5-2 in. in length. Ice-19-22 (LM-MAF) contained a total of 25 scab-like or irregularly shaped specimens that were generally rather small (< 1 gram). Ice-25 (JSC) consisted of 26 slender beams of ~25 grams each of dimensions ~8 in. x 0.8 in. x 0.25 in. Of these, one was curved to conform to the bellows on the LOX feedline. Photographs of most of the specimens are given in Section 4 along with their microstructure.

The ice was prepared in different ways. Ice-15 and Ice-19-22 were grown on the face of a foam-insulated, cryogenically cooled plate at LM-MAF, under simulated atmospheric conditions. Ice-16-18 was prepared at Aerotek-JSC, by either spraying water over frost at regular intervals or compacting frost. In more detail, low-density ice, ranging from 24 lbs/ft^3 to 48 lbs/ft^3 (0.384 g/cc to 0.768 g/cc) was manufactured in the form of rectangular prisms and right cylinders of various dimensions by Hypervelocity Impact Test Facility personnel at JSC. The LD ice projectiles were manufactured on an LN2 cold plate in an environmental chamber that controlled ambient air temperature and humidity. The ambient air temperature was maintained between 45 and 49 °F with a relative humidity ranging from 90 to 95 percent. These ambient conditions, in conjunction with LN2 cold plate temperatures from -275 to -300 °F, were established to simulate the environment of a filled ET during night conditions on the launch pad at KSC. The low-density ice projectiles were grown in Lexan molds by introducing atomized mist from a pump sprayer in layers over many hours until the projectiles achieved the desired thickness. The projectiles were then transferred from the chamber to a walk-in freezer (T = ~12 °F) where they were 'cured' for approximately 8 hours then extracted from the molds, measured and weighed. Depending on the requested projectile dimensions, many projectiles were precisely machined using a flycutter operating between 2500 and 3000 rpm. Finally, Ice-25 was grown by freezing water. Further details, where we know them, are given in Section 4.

With the exception of Ice-18, which was in storage at the time of writing, we characterized each batch of ice. The type of characterization, however, varied from batch-to-batch, as noted in Table 1. Friability impeded the characterization of Ice-17, and size permitted only microstructure, density and a few compression tests on most of the other lots. Ice-25 afforded a more complete characterization. However, the program ended shortly after the shipment arrived, and so we only examined the microstructure of the curved beam from this shipment. The other specimens of this lot were in storage at the time of writing.

3. EXPERIMENTAL PROCEDURES

3.1 Microstructure

We observed the microstructure of the specimens by examining thin-sections under direct light and/or between crossed polarizing filters, following procedures described in Part-I [Schulson et al. 2005]. Under polarized light, the grains exhibited interference colors and could be easily differentiated.

3.2 Density

We measured density in two ways. An immersion method offers the most accurate measure, provided fluid does not invade the pores. We initially employed that procedure because it allows measures to be obtained from the irregularly shaped specimens in several of the lots. We selected n-heptane because of its low density (0.710 g/cc at -10 °C), and weighed specimens both in air

and when suspended in the fluid. From the difference in weight, $W_{Air} - W_{n\text{-}Hept.}$, and from the known densities of air, ρ_{Air}, and of n-heptane, $\rho_{n\text{-}Hept.}$, we computed the density of the specimen from the relationship:

$$\text{density of ice} = \frac{\rho_{n-Hept} W_{Air} - \rho_{Air} W_{n-Hept}}{W_{Air} - W_{n-Hept}} .$$

We termed such values "wet densities" and used the procedure to characterize Ice -15, -16, -19 and -20. We estimated the error in measurement to be ~±1 percent.

The other procedure was to fashion small prisms and to obtain their density from their dimensions and weight in air. We termed such values "dry densities" and estimated the error in measurement to be ~±3 percent. We used this procedure to characterize Ice-20, -21 and -22.

As described below, the wet density of Ice-20 was ~7.7 percent greater than its dry density. We attribute this difference to the invasion by n-heptane into the pores. To eliminate this problem, we considered applying a thin layer of Formvar, as others have done [Druez et al. 1978-9] when examining larger specimens of porous ice. However, that would have raised another issue—namely, the weight of the thin film—which is not a concern with larger specimens of the kind Druez used. Instead, we abandoned the immersion technique and subsequently used only the dry method.

3.3 Compression Tests

Good measurements of compressive strength posed a challenge. We were able to fashion only small specimens (of mm-dimensions) from the atmospheric ice, Ice 20-22. This meant that our usual practice, described in Part-I [Schulson et al. 2005], of pre-loading ice to a fixed stress (~0.1 MPa) for ~15 min. to allow creep-seating against the platens for better alignment was difficult to achieve. The ice failed at stress levels of ~3 MPa (more below), or under loads of around 50 pounds or less. Owing to the insensitivity of the control system on our uniaxial MTS servohydraulic loading frame, we could not in any controlled manner apply loads as small as one or two pounds and hold them. We tried, but after a number of attempts that ended in premature failure of some of our precious few specimens, and also in the destruction of a 2-kip MTS load cell, we abandoned the practice. Instead, we performed the experiments under stroke control without having crept the specimens.

Another challenge was displacement. The dimensions of the atmospheric ice prohibited direct on-the-ice measurement. Instead, we measured the displacement of the actuator. The stroke was calibrated by an MTS technician March 30, 2005, prior to performing the tests. His report is given in Appendix 1. We aimed for a strain rate (defined as the actuator velocity divided by the length of the specimen) of 0.3 s^{-1} and achieved values very close to that (more below).

Despite the concerns of specimen size and of the indirect measure of displacement and hence strain, we are confident that we obtained good results. We observed every test while standing beside the loading system in the cold room, and found that in every case the broken specimen appeared to have been damaged uniformly, suggesting reasonably good alignment.

Loads presented no concern. We measured them by using a 2-kip cell that we purchased from Lebow Products Inc. Using the voltmeter within the MTS 458-controller, we calibrated the cell at -10 °C, the temperature at which we performed the tests, by placing on it masses of known weights over the range 0-100 pounds. Our loads at failure fell within this range, as already noted.

We weighed the masses themselves using Dartmouth postal scales that are calibrated annually. Appendix 2 shows the results of the cell calibration.

We are also confident that we obtained good results from IRL-snow ice. The specimens were larger—cylinder 22 mm in dia. x 60-65 mm in length—and stronger, and so we were able to creep-seat before loading to terminal failure. We measured displacement by mounting a calibrated MTS extensometer to a cane-shaped rod that was attached to the platens and moved apart as the ice was loaded. This was identical to the method used in Part I [Schulson et. al., 2005] to measure displacement. We measured load using a 110-kip MTS cell that was calibrated by an MTS technician March 30, 2005, after we performed the tests. Appendix 3 gives his report. No correction was necessary.

Data were acquired using either a computer-based acquisition system or an oscilloscope. We used the former system (limited to 1000 points/sec) with the snow ice, but found it to be too slow to capture a large amount of data before terminal failure. For tests on the atmospheric ice, we used the latter system.

4. RESULTS AND OBSERVATIONS

4.1 Microstructure and Density

Unless otherwise noted, the smallest division on the scale that accompanies the micrographs in this section is 1 millimeter.

4.1.1 Ice-15

The microstructure of this material was characterized as predominantly equiaxed grains, Figures 1-3. The average grain diameter was ~1 mm. The wet density of the ice was 0.886±0.017 g/cc, Table 2.

4.1.2 Ice-16

The microstructure of Ice-16 was characterized by a mixture of equiaxed and columnar-shaped grains, Figures 4-9. Thin sections oriented perpendicular to the growth direction (parallel to the cold plate) exhibited only equiaxed grains of average diameter ~0.3-0.5 mm (Figs. 4-8). Sections oriented parallel to the growth direction and spaced by ~3 mm exhibited either the equiaxed and columnar mixture (Fig. 9a and 9c), an almost entirely equiaxed microstructure (Fig. 9b), or an entirely columnar structure (Fig. 9d). One parallel section (Fig. 9a) also revealed a chain of equiaxed grains (arrows) that defined an interface between columnar regions, presumably marking different stages of growth. The wet density was 0.880±0.013 g/cc, Table 3.

4.1.3 Ice 17

This shipment contained two kinds of material. One kind, which includes all but one of the specimens we received (specimens 17-135 to 17-140), was produced through a combination of frost accumulation and spraying /misting with water at regular intervals (of the order of two hours). Generally, the greater the interval between sprayings, the greater was the frost accumulation and the lower was the overall density. The other kind, termed manufactured ice, was produced from frost that was consolidated into a dense mass by either pressing or pounding.

Figure 10 shows macroscopic views of the two kinds of material, as seen on two orthogonal sections through the specimens. Specimen 17-138 contained some very large cavities, on the scale of centimeters, plus curved layers that marked the intervals of misting. Figure 11 shows

more clearly the layered macrostructure of 17-138, as seen on the larger face of the specimen. The manufactured ice contained neither of these features. Instead, it contained a few millimeter-sized crystals (light grey tone in the images) dispersed and embedded within the matrix, plus a few shallow indentations that may have been created when we cut the section.

The microstructure of the frost/misted material is shown in Figure 12. Figures 12a and 12b show two views of the microstructure of specimen 17-138 from thin sections cut parallel to the smaller face of the specimen, as seen through a microscope (hence the round image) through crossed-polarizing filters. Figure 12c shows a four-fold magnified image of the same general area. Figure 12d shows the structure within a section cut perpendicular to the other sections. The images on the two orthogonal sections appear to be almost identical, implying that the microstructure is reasonably isotropic. It may be characterized as a predominantly granular or equiaxed aggregate that contains a small fraction of columnar-shaped grains. The grain size was about 0.1 mm in diameter. In comparison, the diameter of the columnar-grained hard ice described in Part-I [Schulson et al. 2005] was 6-10 mm.

The other features we found within the frost/misted material were tiny pores (0.01 to 0.02 mm dia.) that constituted about 10 to 15 percent of the volume of the material. They are evident from the "black spots" that can be seen by zooming in on any of the images in Figure 12. The pores imparted a milky appearance to the thin sections, owing to the scattering of light. Also, they led to a density of 0.730 g/cc, Table 4, compared with 0.917 g/cc for fully-dense hard ice. The density we measured, incidentally, was significantly greater than the density of 0.580 g/cc obtained by Aerotek-JSC for the same 17-138 material. The reason for the difference, we think, is that our specimen was smaller than the one used by JSC and thus contained fewer cm-sized cavities.

In comparison, the manufactured ice was even more finely structured, Figure 13. (The images were obtained using non-polarized illumination.) The microstructure is composed of equiaxed grains about 0.05 mm in diameter. The grain boundaries lacked cohesion, as evident from the popping out of grains. For that reason we could not get a section thin enough to view through crossed polarizers for interference colors. Again, the ice contained a considerable degree of porosity. In this case, we could not make a quantitative estimate owing to the fine scale of the microstructure. It was apparent, however, that instead of being incorporated primarily within the volume of the grains, as they were in the frost/misted material, the pores appeared to be located primarily at the grain boundaries, thereby accounting for the ease with which the grains popped out when preparing sections. The density of the material was 0.730 g/cc, Table 4.

4.1.4 IRL Snow Ice

Ice-17 was the most finely-grained material that we had examined to date in the Return-to-Flight program. To determine whether we could reproduce it in the Ice Research Laboratory at Dartmouth, we collected some dry snow (whose temperature was 5-10 °F during collection) following a January '05 storm, and then consolidated the snow into 22 mm dia. cylinders by packing it into a thin-walled plexiglass tube. We varied the degree of packing, from low to medium (tapped the snow with a 2 lb. aluminum rod) to high (rammed the snow with the rod). We then allowed the specimens to sinter for 3 days at -10 °C. Subsequently, we warmed the sides of the plastic tube to release the ice, Figure 14, and then examined the microstructure. Once again, the ice was very finely grained, Figure 15: ~0.1 mm dia. after the low and medium degrees of consolidation (Figs. 15a,b) and ~0.06 mm after the high degree (Fig. 15c). The ice was also highly porous, especially after only a low degree of packing. In that case, the individual grains sintered together only moderately well. (The microstructure can be best seen by zooming in on the images.) The density was low, but increased from 0.170±0.020 g/cc for the most lightly packed aggregate to 0.560 g/cc for the most heavily packed, Table 5. The density of our most highly compacted/sintered material was almost the same as the density of the manufactured ice from Aerotek-JSC (0.570 g/cc, Table 4).

It appears, therefore, that the frost/snow/compaction process reproducibly generates finely-grained, porous material.

4.1.5 Ice-18

This shipment contained 13 cylindrically shaped specimens of dimensions and weight listed in Table 6. Of these, six had been made by compacting frost. The others were made from frost plus misting, in the manner of Ice-17. The intention was to measure the compressive strength of both materials. That was not done. The loading system was in need of maintenance, and by the time the repairs were made and the system was calibrated the focus of the program had changed. The ice was in storage at Dartmouth in the Ice Research Lab at the time of writing.

4.1.6 Ice-19

This shipment contained five cm-sized pieces of atmospheric ice. The material had been made on March 3, 2005 at LM-MAF, by forming on the face of a cryogenically cooled plate under the following atmospheric conditions: 55 °F, 90 percent relative humidity, solar heating throughout the growth period, and simulated wind after ~4 hours of accumulation. The solar heating was set at 80 BTU/hr ft^2 and the wind was set at approximately 5 knots. We examined the microstructure from thin-sections taken parallel to the largest face of each sample, and determined the wet density of the ice at -10 °C.

Figures 16-20 show the five specimens and their microstructures, as seen from thin-sections taken parallel to the cold plate; missing is the structure of specimen 2E1-3/5/05 because the sample was fractured into pieces too small to easily examine. All specimens were cloudy in appearance, implying the presence of porosity. The level, however, was relatively low, for the wet density of the ice was relatively high at 0.894±0.020 g/cc, Table 7. From the values listed there, and assuming the pores were air-filled, the porosity ranged from as low as 0.3 percent by vol. to 5.5 percent. The microstructure confirmed these values. Very few pores were present in specimen 2E2-3/5/05, the most dense sample, and many of the grains appeared to be pore-free (Fig. 20b). In comparison, the least dense sample, specimen 241-3/5/05, contained many more

pores, and a more uniform distribution of them, as evident from the spots on the micrograph (Fig. 16b).

The microstructure was mixed. Specimens 2B1-3/5/05 and 2E2-3/5/05 contained both equiaxed and columnar-shaped grains (Figs. 17b and 20b): the dimensions of the largest ones were between 5 and 10 mm; the smallest grains were of a sub-millimeter size. Within the other two samples we examined, 241-3/5/05 and 2B2-3/5/05, the grains were more equiaxed in shape, and smaller: the largest ones were between 1 and 2 mm in dia. while the smallest grains, which dominated, were between 0.1 and 0.3 mm.

4.1.7 Ice-20

We received eight small pieces of ice from LM-MAF. They, too, were harvested from the face of a cryogenically cooled plate that had been exposed to the following atmospheric conditions on March 7, 2005: 85 °F and 80 percent relative humidity. Neither wind nor solar heat was applied. We examined the microstructure, determined the density of the ice at -10 °C using both the wet and dry methods, and measured the compressive strength.

Figures 21-28 show the specimens and their microstructure. In this series, the thin-sections from which the microstructure was recorded were generally oriented perpendicular to the plane of the cold plate. When the orientation was of that kind, "foam side" is shown on the micrograph. Again, the ice was cloudy in appearance, owing to pores incorporated within the structure. The average level of porosity was about the same as it was in Ice-19, as evident from the fact that the average wet density of the set, Table 8, was essentially the same as the wet density from Ice-19; namely, 0.897±0.007 g/cc vs 0.894±0.020 g/cc.

Once again, the microstructure was composed of a relatively fine mixture of equiaxed and columnar-shaped grains. Of particular note is the layered structures: layers of fine crystals (~0.1 mm < d < 1 mm) separated layers of columnar-shaped grains of larger size (up to ~5 mm) and of lower porosity than the aggregate as a whole. When viewed in direct light, as shown in Fig. 21c, the layers in specimen 2E1-3/7/05 appear to have delaminated, judging from the contrast in the image. However, when examined in polarized light, Fig. 21 b, it became clear that that ice had not delaminated. The material was simply bubble-free in certain bands, which caused the contrast in the direct image.

4.1.8 Ice-21

This shipment contained seven small pieces of ice, again from LM-MAF. As in the cases of Ice-19 and Ice-20, each piece had been harvested from the face of a cold plate insulated with foam. The material was grown March 14, 2005 under transient, no-wind conditions which started at 70 °F and 95 percent relative humidity, and then changed after about four hours of accumulation to 85 °F and 60 percent relative humidity. Solar heating was applied. We examined the microstructure, measured the dry density of the ice at -10 °C, and measured the compressive strength.

Figures 29-35 show the specimens and their microstructure. These samples were as cloudy as the earlier ones, for the same reason. The structures were again viewed from thin-sections that were taken perpendicular to the plane of the plate. In this series, we include not only the structure as seen through polarizing filters, but also as seen through direct light. The latter condition exposes the pores more clearly. When certain of the side that contacted the foam, we noted it on the micrographs, as before. The dry density of Ice-21 was 0.823±0.044 g/cc, Table 9, essentially the same as the dry density of Ice-20, which was 0.828±0.036 g/cc.

The microstructure once again was characterized by a mixture of fine (d ~ 0.3 mm) equiaxed grains and coarse (up to ~10 mm) columnar-shaped grains.

4.1.9 Ice-22

This shipment was the last one we received that contained specimens that had been harvested from the face of a cold plate at LM-MAF. It contained five pieces, still small but somewhat larger than the samples from Ice-19-21. The ice was grown on March 16, 2005 under the following atmospheric conditions: 55 °F, 90 percent relative humidity, with solar heating throughout the test plus simulated wind after about four hours of accumulation. We examined the microstructure under both direct and polarized light, measured the dry density at -10 °C and measured the compressive strength.

Figures 36-40 show the specimens and their microstructure as viewed from thin-sections taken parallel to their largest face. The parallel sets of lines on the direct-light images are not microstructural features, but are marks from the band-saw blade we used to prepare the sections. The specimens were again cloudy in appearance. The dry density was 0.846±0.060 g/cc, Table 10.

Once again the microstructure was characterized by a mixture of equiaxed and columnar-shaped grains, as well as porosity. Specimen 2E1-3/16/05 contained some very coarse grains (~5 mm x 10 mm), Fig. 36c, as did specimen 2E2-3/16/05, Fig. 37c. Particularly striking in these samples was the association of the more finely-grained regions of the microstructure with regions of greater porosity, evident from the bands of pores and of very fine grains (d ~ 0.3 mm) in specimen 2E3-3/16/05, Fig. 38, and specimen 2BSTRA1-3/16/05, Fig. 39.

In a general sense, the microstructure of Ice-22 was similar to the structure of Ice 19-21. So, too, was the density when compared on the same basis. This is not surprising, given that the ice in each of these cases was prepared in essentially the same manner under similar atmospheric conditions.

4.1.10 Ice-25

This was the last shipment we received. It contained 26 specimens shaped as slender beams ~8 in. x 1 in. x 1/4 in. Of these, 25 beams were straight; the other one was curved in the shape of the bellows on the shuttle fuel line, as sketched in Fig. 41a. Fig. 41b shows plan views (along direction-Z of Fig. 41a) of both a straight and the curved beam, and Fig. 41c illustrates the thickness of the beams. Four straight beams (Group-A, Table 1) were made quickly by pouring distilled water into a cold (~0 °F) aluminum mold set in a freezer whose temperature varied from -5 to +5 °F. Solidification occurred within ~15 min. Four other beams (3 straight and 1 curved, Group B) were made from boiled distilled water, in an attempt to reduce porosity. The water was poured into an aluminum mold and then placed in a freezer at ~0 °F. Freezing occurred within about 1 hour. The other 18 straight beams (Groups C-F, termed "normal", Table 1) were made by pouring distilled water at room temperature into an aluminum mold at the same temperature, and then by placing the filled mold in a freezer at ~0 °F. Complete freezing occurred within 1.5 hours. We examined the microstructure of the single curved beam. At the time of writing, the others are in storage in the IRL.

Figure 42 shows six photographs of the structure of the curved beam. In comments below we refer to sections XZ and YZ, where X,Y and Z define a right-handed co-ordinate system, shown in Fig. 41a. Section XZ defines a transverse cross-section. Section YZ defines a longitudinal cross-section. When viewed along the Z-direction, Fig. 42a, the ice exhibited a mixture of fine

(approx. mm-sized, left side) and coarse (several mm) grains. An XZ transverse section, Fig. 42b, revealed finer grains and a bubble-rich boundary along the mid-plane of the beam. Another XZ transverse section, Fig. 42c, showed a large pancake-shaped grain plus other grains of several mm's diameter. Fig. 42d is a direct light image that shows the bubble-rich centerline noted in Figs. 42b and 42c. Fig. 42e shows a mixture of fine (~1 mm) and coarse (~ several mm) grains as seen in a YZ longitudinal section from the middle of the bar. Finally, Fig. 42f shows again the center-plane of bubbles, as seen in a YZ longitudinal section.

The presence of the bubble-rich center-plane clearly shows that the ice grew in the Z-direction, both top down and bottom up, and that the rate of growth was about the same in the two directions. This growth character is also evident in the somewhat elongated grains (along Z) seen in Figs 42b and 42e.

4. 2 Uniaxial Compressive Strength

Whether originating from water in the atmosphere (Ice 20-22) or by consolidating snow, the ice behaved in a brittle manner in every test. The failure mode appeared to be a combination of splitting along the loading direction plus shear faulting. In other words, the soft ice behaved very much like the hard ice described in Part-I [Schulson 2005].

Again, test data as well as stress-time and displacement-time plots are given on the JSC website. Strain may be obtained from the displacement and from the length of the specimen. Also included on the website are photographs of most of the specimens, taken both before and after testing. Figures 43 and 44 show examples of snow ice and atmospheric ice, respectively, before and after testing.

Table 11 summarizes the failure stress of the atmospheric ice, along with specimen dimensions. The strength corresponds to the highest stress recorded during each test. The data are too few to draw firm conclusions about possible variations from batch-to-batch. However, Ice-22 appears to be stronger. The most likely explanation is the clarity of the test specimens: while the parent piece of ice was essentially of the same density as Ice-20 and Ice-21, the actual test specimens of Ice-22 were generally cut from the clearer parts of the parent that contained fewer bubbles. This point is noted in the data files under "overview". For comparison, Table 12 lists the strength of the snow ice.

5. DISCUSSION

5.1 Brittle Compressive Strength

Table 13 summarizes the present measurements. While there is little in the data to distinguish one batch of atmospheric ice from another (Ice-20 -22), the data clearly show that the more porous (snow) ice is the weaker material, despite its finer microstructure. Considering its finer microstructure, it should have had a higher strength. This suggests that what might have been added to strength by the finer grains [Schulson 2001] was more than taken away by the stress-concentrating effect of the pores.

In comparison, the strength of "hard", coarsely-grained (d = 8±2 mm) columnar ice, when loaded along the columns at the same temperature (-10 °C) and strain rate (~0.3 s^{-1}), was 11.0±1.7 MPa and the strength of single crystals (-10 °C, 0.01 s^{-1}) was 14.8±2.3 MPa [Schulson et al. 2005]. The soft ice we examined here was weaker (1.4 – 6.3 MPa) than the hard ice we examined earlier by a factor of 2-5.

How well do the present results compare with earlier measurements? The literature contains a paucity of data on the mechanical properties of atmospheric ice, and so in-depth comparisons cannot be made. However, the work of Druez et al. [1978-79, 1986, 1987] is informative. They prepared equiaxed, polycrystalline specimens of grain size between 0.5 and 1 mm and of a range of density (~0.680-0.917 g/cc), and measured the compressive strength at temperatures between -2 and -15 °C at strain rates between 10^{-5} s^{-1} and 0.04 s^{-1}. At the highest strain rate, the ice exhibited brittle behavior and so can be compared with the present results. Although scattered, their data indicate that the brittle compressive strength generally decreased with decreasing density and with increasing temperature. At -10 °C, it fell from ~8 MPa near full density to ~1 MPa at a density of ~0.740 g/cc. For densities comparable to those of Ice 20-22, the strength varied from ~2.5 MPa to ~4 MPa. It would appear, therefore, that the present results are in reasonable agreement with earlier ones, despite the fact that they were obtained at a higher strain rate (0.3 s^{-1} vs 0.04 s^{-1}) which could have imparted a very small increment of strength, as discussed in Part-1 [Schulson et al. 2005).

5.2 Tensile Strength

Owing to limitations in the amount of ice available to us and to the size of the samples, we were unable to measure the tensile strength of the ice. However, for guidance we turn again to Druez et al. [1987]. They measured tensile strength vs density (~0.830-0.917 g/cc) at -8 and -20 °C. They found that temperature, unlike its effect on brittle compressive failure, has little effect on tensile strength, in agreement with the behavior of hard ice [Schulson 2001]. Again, their data are scattered. Yet over the range of density examined a trend could not be seen. The strength varied from a low value of ~0.5 MPa to a high value of ~2.8 MPa. Druez et al. [1987] commented that the tensile strength was lower than the compressive strength by a factor of 2-5. Note that the upper limit on tensile strength is greater by about a factor of two than the tensile strength of nearly fully-dense granular ice of 1 mm grain size [Schulson et al. 1984], owing most likely to the finer grain size. Given that our compressive strengths are in reasonable agreement with those of Druez et al., it seems fair to assume that the tensile strength of the present material was probably between ~0.5 and 2 MPa. These values can be used for modeling purposes in the absence of actual test data.

5.3 Young's Modulus and Poisson's Ratio

Also of interest is elastic behavior. Again we turn to the literature, because we did not make such measurements during the present study. Keller et al. [1999] summarize both Young's modulus, E, and Poisson's ratio, ν, of porous ice, Figure 45. In that figure the degree of porosity is defined by the relationship $\phi = 1 - \rho/\rho_{th}$ where ρ and ρ_{th}, respectively, are the density of porous ice and the density of pore-free material. The original data were obtained from ultrasonic studies of the transformation of snow to ice within glaciers, by Bentley et al. [1957] and by Brockamp and Pistor [1969], and from measurements on ice shelves by Thiel and Ostenso [1961], and the data agree well with those of Shapiro et al. [1997]. The data in the figure apply to relatively warm ice. Temperature, however, has only a small effect on the stiffness of ice [Gammon et al. 1983]—Young's modulus increases by only about 5 percent between 0 and -50 °C—and so the measurements are relevant to the present study. Static moduli may be lower than the dynamic moduli given in Figure 45.

Poisson's ratio is relatively independent of porosity, at least up to $\phi \sim 0.6$ where the data end. A good value is $\nu = 0.3$. Young's modulus, on the other hand, decreases significantly with increasing porosity/decreasing density. For material of the density of Ice-19-22, for which $\phi \sim 0.1$, the modulus has the value E ~7.0±0.5 GPa. This compares with the value E = 9.3 GPa for fully dense ice at -16 °C [Gammon et al. 1983]. In other words, porosity has a smaller effect on the stiffness of ice than on its strength.

5.4 Final Comments

While we attempted in this investigation to improve our knowledge and understanding of low-density ice, we recognize that more work is needed before a complete picture emerges. Of particular need is a systematic study of the role of porosity per se on the inelastic behavior of material of constant grain size, where the range of porosity extends to the lowest limits. Similarly, a study of grain size effects on low-density ice of constant porosity is also needed. Fabrication of material with a reproducible microstructure poses a significant challenge here. However, with experience gained from the present study, we think that that obstacle can be overcome. Perhaps the simplest method to pursue is to consolidate snow crystals of different sizes, say by controlled extrusion. While that process would not simulate the columnar-shaped constituent of some variants, we think that that shortcoming would be more than balanced by the contolled granular constituent. As the present study revealed, the pores reside more within the granular constituent than within the columnar component of low-density atmospheric ice.

6. CONCLUSIONS

From a study of the microstructure, the density and the compressive strength at -10 °C at ~0.3 s^{-1} of porous ice, produced from both atmospheric water and consolidated snow, we conclude that:

(i) the atmospheric material was generally composed of a mixture of very fine (0.1-0.3 mm) and coarse (5-10 mm) grains, plus air bubbles distributed preferentially within the more finely-grained part of the microstructure;

(ii) the snow ice was composed of even finer grains (~0.05 mm) and of more pores;

(iii) correspondingly, the snow ice was of lower density than the atmospheric ice and both were significantly less dense than hard ice; and

(iv) the atmospheric ice was stronger than the snow ice, but weaker by a factor of 2-5 than pore-free hard ice examined in Part I. This soft ice ranged in compressive strength from 1.4 to 6.3 MPa;

(v) mechanical properties of the soft ice were estimated from knowledge of the microstructure and studies from the literature. The tensile strength was estimated to be between 0.5 and 2 MPa, Young's modulus between 3 and 8 GPa depending on density, and Poisson's ratio of 0.3.

7. Appendices

7.1 Calibration of MTS actuator stroke

MTS Systems Corporation

14000 Technology Drive
Eden Prairie, MN 55344-2290

A2LA Certificate 1145.01

MTS Field Service

Certificate of Calibration

Page: 1 of 1

Customer Name: Dartmouth College
Certificate Number: 2456-414
System: 931-10
Site: 505453
System ID: 505453
Location:
Country Code: USA

Equipment

Device Type: Length
Model: LVDT
Serial No.: 137
Controller/Conditioner Model: 458-13
Serial No.: 0157351
Readout Device Model: 458.20
Serial No.: 0110128
Channel: xdcr#1

MTS Field Service is accredited by the American Association for Laboratory Accreditation (A2LA Cert. No. 1145.01). The basis for this accreditation is the international standard for calibration laboratories, ISO/IEC 17025 "General Requirements for the Competence of Calibration and Testing Laboratories".

Defined and documented measurement assurance techniques or uncertainty analyses are used to verify the adequacy of the measurement processes. These techniques or analyses are available upon request.

Calibrations are performed with standards whose values and measurements are traceable to the National Institute of Standards and Technology.

CALIBRATION INFORMATION

As Found: In Tolerance Max. Error As Found: 0.65 % Calibration Date: 30-Mar-05
As Left: In Tolerance Max. Error As Left: 0.65 % Calibration Due: 30-Mar-06
Tolerance: +/-1.0% of Range
Calibration Procedure: FS-CA 2104 Rev. D
Full Scale Ranges: 3 inch, .6 inch
Note:

STANDARDS USED FOR CALIBRATION

MTS Asset Number	Manufacturer	Model Number	Description	Cal. Date	Cal. Due
12653	Fluke	80T-150U	Temperature Probe	15-Dec-03	15-Dec-05
17589	CDI	BG2820	CDI	27-Jun-04	27-Jun-05

Certified by: Dave Sch

Issued on: 30-Mar-05

MTS Systems Corporation
14000 Technology Drive
Eden Prairie, MN 55344-2290

Calibration Report

 A2LA Certificate 1145.01

Customer Name: Dartmouth College — Report Number: 2456-414
System: 931-10 — Site: 505453
System ID: 505453 — Location: — Country Code: USA

Equipment
Device Type: Length — Model: LVDT — Serial No.: 137
Controller/Conditioner Model: 458-13 — Serial No.: 0157351
Readout Device Model: 458.20 — Serial No.: 0110128 — Channel: xdcr#1

Procedure
MTS Procedure: FS-CA 2104 Rev. D
Calibration has been performed in accordance with: (none)
Method of Verification:

Calibration Equipment Asset No.
Dead Weight Set: — HighLevel Board: — LowLevel Board: — Standard Asset No.: 17589
DW Compensation: — DMM: — Digital Indicator: — Lower Limit:
Temperature Readout: 12653 — Additional Equipment: — Standardizer:

Conditions
Ambient Temperature: 65.00 °F — Polarity(+): Retraction — Bidirectional: — Cable Length: 30 Feet

In Tolerance	X	**As Found:**	X	**Tolerance: +/-1.0% of Range**
Out of Tolerance		**As Adjusted:**		**As Found System Condition:** Good

Conditioner Parameters
Excitation: — Delta K: — Zero Offset: — Multiplier: — Phase:
Cal Factor: Positive: — Negative: — PreAmp Gain: — FineGain:

Calibration Data

Extension **Range:** 1 **Full Scale:** 3
Report Units: inch

Applied Length Percent	Series 1 Indicated Reading Ascending	Series 1 Indicated Reading Descending	Series 1 Errors Units Error Asc	Series 1 Errors Percent Error Asc	Series 1 Errors Units Error Desc	Series 1 Errors Percent Error Desc	Series 2 Indicated Reading Ascending	Series 2 Indicated Reading Descending	Series 2 Errors Units Error Asc	Series 2 Errors Percent Error Asc	Series 2 Errors Units Error Desc	Series 2 Errors Percent Error Desc	Repeatability Percent Error Asc	Repeatability Percent Error Desc
0	0.00000	0.00000	0.00	0.00	0.00	0.00								
-20	-0.60040		0.00	0.01										
-40	-1.19520		0.00	-0.16										
-60	-1.78120		0.02	-0.63										
-80	-2.38710		0.01	-0.43										
-100	-2.99040		0.01	-0.32										

Retraction **Range:** 1
Report Units: inch

Applied Length Percent	Series 1 Indicated Reading Ascending	Series 1 Indicated Reading Descending	Series 1 Errors Units Error Asc	Series 1 Errors Percent Error Asc	Series 1 Errors Units Error Desc	Series 1 Errors Percent Error Desc	Series 2 Indicated Reading Ascending	Series 2 Indicated Reading Descending	Series 2 Errors Units Error Asc	Series 2 Errors Percent Error Asc	Series 2 Errors Units Error Desc	Series 2 Errors Percent Error Desc	Repeatability Percent Error Asc	Repeatability Percent Error Desc
0	0.00000	0.00000	0.00	0.00	0.00	0.00								
20	0.60049		0.00	0.02										
40	1.19190		0.01	-0.27										
60	1.78910		0.01	-0.36										
80	2.39210		0.01	-0.26										
100	2.99850		0.00	-0.05										

Errors at Zero are computed in % of Range.
The resolution of this Data Set is reflected in the least significant digit reported.
Uncertainty of the data supplied is equal to or less than +/-0.25% of reading for a confidence level of 95%.
This report shall not be reproduced except in full, without the written approval of the laboratory.
Calibrations are performed with standards whose values and measurements are traceable to the National Institute of Standards and Technology.
American Association of Laboratory Accreditation Certificate Number: 1145.01
Notes:

Out of Tolerance in % column

Performed By: Dave Salow — Field Service Engineer — Date: 30-Mar-05

Signature: Dave Salow — Next Customer Agreed Upon Calibration Date: 30-Mar-06 — ACSRep0016

MTS Systems Corporation
14000 Technology Drive
Eden Prairie, MN 55344-2290

Calibration Report

A2LA Certificate 1145.01

Customer Name: Dartmouth College
Report Number: 2456-414
System: 931-10
Site: 505453
System ID: 505453 Location:
Country Code: USA

Equipment
Device Type: Length Model: LVDT Serial No.: 137
Controller/Conditioner Model: 458-13 Serial No.: 0157351
Readout Device Model: 458.20 Serial No.: 0110128 Channel: xdcr#1

Procedure
MTS Procedure: FS-CA 2104 Rev. D
Calibration has been performed in accordance with: (none)
Method of Verification:

Calibration Equipment Asset No.
Dead Weight Set: HighLevel Board: LowLevel Board: Standard Asset No.: 17589
DW Compensation: DMM: Digital Indicator: Lower Limit:
Temperature Readout: 12653 Additional Equipment: Standardizer:

Conditions
Ambient Temperature: 65.00 °F Polarity(+): Retraction Bidirectional: Cable Length: 30 Feet

In Tolerance	X	**As Found:**	X
Out of Tolerance		**As Adjusted:**	

Tolerance: +/-1.0% of Range
As Found System Condition: Good

Conditioner Parameters
Excitation: Delta K: Zero Offset: Multiplier: Phase:
Cal Factor: Positive: Negative: PreAmp Gain: FineGain:

Calibration Data
Extension **Range:** 2 **Full Scale:** 0.6
Report Units: inch

Applied Length Percent	Series 1 Indicated Reading Ascending	Series 1 Indicated Reading Descending	Series 1 Errors Units Error Asc	Series 1 Errors Percent Error Asc	Series 1 Errors Units Error Desc	Series 1 Errors Percent Error Desc	Series 2 Indicated Reading Ascending	Series 2 Indicated Reading Descending	Series 2 Errors Units Error Asc	Series 2 Errors Percent Error Asc	Series 2 Errors Units Error Desc	Series 2 Errors Percent Error Desc	Repeatability Percent Error Asc	Repeatability Percent Error Desc
0	0.00000	0.00000	0.00	0.00	0.00	0.00								
-20	-0.11893		0.00	-0.18										
-40	-0.23852		0.00	-0.25										
-60	-0.36020		0.00	0.03										
-80	-0.48170		0.00	0.28										
-100	-0.60393		0.00	0.65										

Retraction **Range:** 2
Report Units: inch

Applied Length Percent	Series 1 Indicated Reading Ascending	Series 1 Indicated Reading Descending	Series 1 Errors Units Error Asc	Series 1 Errors Percent Error Asc	Series 1 Errors Units Error Desc	Series 1 Errors Percent Error Desc	Series 2 Indicated Reading Ascending	Series 2 Indicated Reading Descending	Series 2 Errors Units Error Asc	Series 2 Errors Percent Error Asc	Series 2 Errors Units Error Desc	Series 2 Errors Percent Error Desc	Repeatability Percent Error Asc	Repeatability Percent Error Desc
0	0.00000	0.00000	0.00	0.00	0.00	0.00								
20	0.12089		0.00	0.15										
40	0.24102		0.00	0.17										
60	0.36060		0.00	0.10										
80	0.48221		0.00	0.37										
100	0.60332		0.00	0.55										

Errors at Zero are computed in % of Range.
The resolution of this Data Set is reflected in the least significant digit reported.
Uncertainty of the data supplied is equal to or less than +/-0.25% of reading for a confidence level of 95%.

Calibrations are performed with standards whose values and measurements are traceable to the National Institute of Standards and Technology.
American Association of Laboratory Accreditation Certificate Number: 1145.01
Out of Tolerance in % column
Notes:

Performed By: Dave Salow Field Service Engineer Date: 30-Mar-05

Signature:

Next Customer Agreed Upon Calibration Date: 30-Mar-06 ACSRep0016

Appendix 7.2 Calibration of the Lebow 2-kip load cell

weight [lbs]	reading [V]
0	0
10	0.064
20	0.125
30	0.188
40	0.252
50	0.315
70	0.445
90	0.572
95	0.601
100	0.631

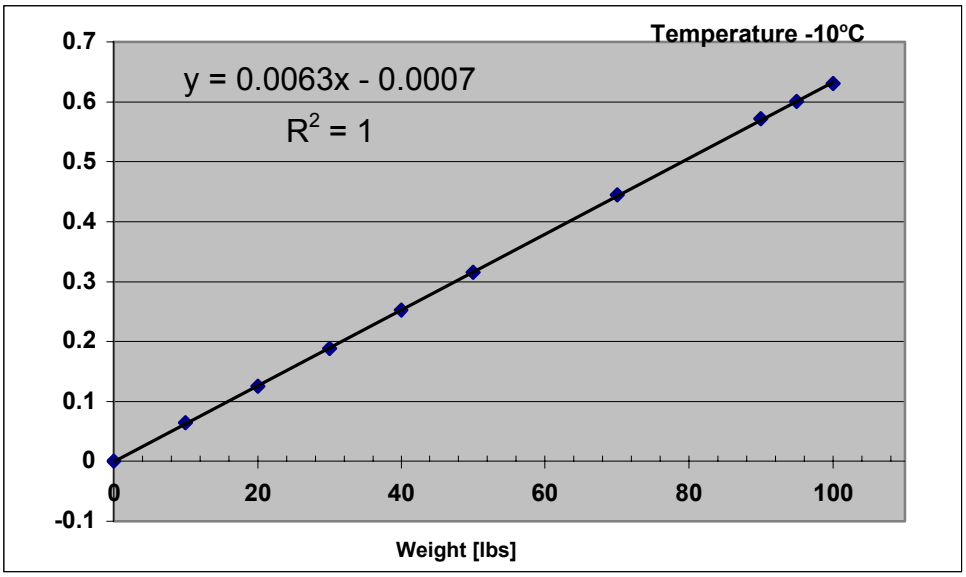

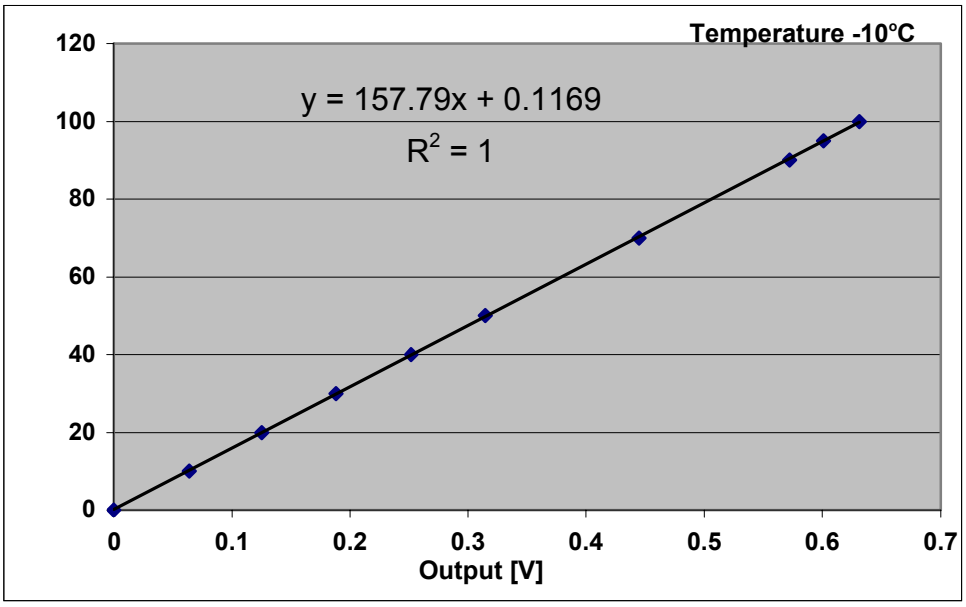

Appendix 7.3 Calibration of 110 kip MTS load cell

MTS Systems Corporation

14000 Technology Drive
Eden Prairie, MN 55344-2290

A2LA Certificate 1145.01

MTS Field Service

Certificate of Calibration

Customer Name: Dartmouth College
Certificate Number: 2456-415
System: 931-10
Site: 505453
System ID: 505453
Location:
Country Code: USA

Equipment

Device Type: Force — Model: 661.23A-02 — Serial No.: 1657
Controller/Conditioner Model: 458-11 — Serial No.: 100999
Readout Device Model: 458_20_READOUT — Serial No.: 0110128 — Channel: xdcr#2

MTS Field Service is accredited by the American Association for Laboratory Accreditation (A2LA Cert. No. 1145.01). The basis for this accreditation is the international standard for calibration laboratories, ISO/IEC 17025 "General Requirements for the Competence of Calibration and Testing Laboratories".

Defined and documented measurement assurance techniques or uncertainty analyses are used to verify the adequacy of the measurement processes. These techniques or analyses are available upon request.

Calibrations are performed with standards whose values and measurements are traceable to the National Institute of Standards and Technology.

CALIBRATION INFORMATION

As Found: In Tolerance — Max. Error As Found: 0.38 % — Calibration Date: 30-Mar-05
As Left: In Tolerance — Max. Error As Left: 0.38 % — Calibration Due: 30-Mar-06
Tolerance: +/-1.0% of Applied Force
Calibration Procedure: FS-CA 2103 Rev. D
Full Scale Ranges: 100000 lbf, 10000 lbf
Note:

STANDARDS USED FOR CALIBRATION

MTS Asset Number	Manufacturer	Model Number	Description	Cal. Date	Cal. Due
16999	Interface Inc.	9840	Readout	1-Dec-04	1-Dec-05
12653	Fluke	80T-150U	Temperature Probe	15-Dec-03	15-Dec-05
16674	Interface	CX-0220-1	Bridge simulator	11-Oct-04	11-Oct-05
14223	Revere	100 Kip	100 Kip standard	28-Jul-04	28-Jul-05

Certified by: [signature] Issued on: 30-Mar-05

MTS Systems Corporation
14000 Technology Drive
Eden Prairie, MN 55344-2290

Calibration Report

Page: 1 of 2 A2LA Certificate 1145.01

Customer Name: Dartmouth College
Report Number: 2456-415
System: 931-10 Site: 505453
System ID: 505453 Location: Country Code: USA

Equipment
Device Type: Force Model: 661.23A-02 Serial No.: 1657
Controller/Conditioner Model: 458-11 Serial No.: 100999
Readout Device Model: 458_20_READOUT Serial No.: 0110128 Channel: xdcr#2

Procedure
MTS Procedure: FS-CA 2103 Rev. D
Calibration has been performed in accordance with: ASTM E4-02
Method of Verification: Set-the-Force Method using Elastic Calibration Devices

Calibration Equipment Asset No.
Dead Weight Set: HighLevel Board: LowLevel Board: Standard Asset No.: 14223
DW Compensation: DMM: Digital Indicator: 16999 Lower Limit: 5743 lbf
Temperature Readout: 12653 Additional Equipment: Standardizer: 16674

Conditions
Ambient Temperature: 65.00 °F Polarity(+): Tension Bidirectional: Cable Length: 50 Feet Feet

In Tolerance	X	**As Found:**	X	**Tolerance: +/-1.0% of Applied Force**	
Out of Tolerance		**As Adjusted:**		**As Found System Condition:**	**Good**

Conditioner Parameters
Excitation: 8.5000 Delta K: Zero Offset: Multiplier: Cal Res: kohms
Shunt Cal: Positive: Negative: PreAmp Gain: FineGain:

Calibration Data
Compression **Range:** 1 **Full Scale:** 100000
Report Units: lbf

	Series 1		Series 1 Errors				Series 2		Series 2 Errors				Repeatability
Applied Force Percent	Indicated Reading Ascending	Indicated Reading Descending	Units Error Asc	Percent Error Asc	Units Error Desc	Percent Error Desc	Indicated Reading Ascending	Indicated Reading Descending	Units Error Asc	Percent Error Asc	Units Error Desc	Percent Error Desc	Percent Error Asc	Percent Error Desc
0	0.0	0.0	0.00	0.00	0.00	0.00	0.0	0.0	0.00	0.00	0.00	0.00	0.00	0.00
-20	-20075.0		75.00	0.38			-20032.0		32.00	0.16			0.22	
-40	-40031.0		31.00	0.08			-40013.0		13.00	0.03			0.05	
-60	-60048.0		48.00	0.08			-60093.0		93.00	0.16			0.08	
-80	-80024.0		24.00	0.03			-80115.0		115.00	0.14			0.11	
-100	-100020.0		20.00	0.02			-100130.0		130.00	0.13			0.11	

Tension **Range:** 1
Report Units: lbf

	Series 1		Series 1 Errors				Series 2		Series 2 Errors				Repeatability
Applied Force Percent	Indicated Reading Ascending	Indicated Reading Descending	Units Error Asc	Percent Error Asc	Units Error Desc	Percent Error Desc	Indicated Reading Ascending	Indicated Reading Descending	Units Error Asc	Percent Error Asc	Units Error Desc	Percent Error Desc	Percent Error Asc	Percent Error Desc
0														
20														
40														
60														
80														
100														

Errors at Zero are computed in % of Range.
The resolution of this Data Set is reflected in the least significant digit reported.
Uncertainty of the data supplied is equal to or less than +/-0.25% of reading for a confidence level of 95%.
This report shall not be reproduced except in full, without the written approval of the laboratory.
Calibrations are performed with standards whose values and measurements are traceable to the National Institute of Standards and Technology.
American Association of Laboratory Accreditation Certificate Number: 1145.01
Out of Tolerance in % column

Notes:

Performed By: Dave Salow Field Service Engineer Date: 30-Mar-05

Signature:

Next Customer Agreed Upon Calibration Date: 30-Mar-06 ACSRep0016

MTS Systems Corporation
14000 Technology Drive
Eden Prairie, MN 55344-2290

Calibration Report

A2LA Certificate 1145.01

Customer Name: Dartmouth College
Report Number: 2456-415
System: 931-10
Site: 505453
System ID: 505453 Location:
Country Code: USA

Equipment

Device Type: Force Model: 661.23A-02 Serial No.: 1657
Controller/Conditioner Model: 458-11 Serial No.: 100999
Readout Device Model: 458_20_READOUT Serial No.: 0110128 Channel: xdcr#2

Procedure

MTS Procedure: FS-CA 2103 Rev. D
Calibration has been performed in accordance with: ASTM E4-02
Method of Verification: Set-the-Force Method using Elastic Calibration Devices

Calibration Equipment Asset No.

Dead Weight Set: HighLevel Board: LowLevel Board: Standard Asset No.: 14223
DW Compensation: DMM: Digital Indicator: 16999 Lower Limit: 5743 lbf
Temperature Readout: 12653 Additional Equipment: Standardizer: 16674

Conditions

Ambient Temperature: 65.00 °F Polarity(+): Tension Bidirectional: Cable Length: 50 Feet Feet

In Tolerance	X	**As Found:**	X	**Tolerance: +/-1.0% of Applied Force**
Out of Tolerance		**As Adjusted:**		**As Found System Condition:** Good

Conditioner Parameters

Excitation: 8.5000 Delta K: Zero Offset: Multiplier: Cal Res: kohms
Shunt Cal: Positive: Negative: PreAmp Gain: FineGain:

Calibration Data

Compression **Range:** 2 **Full Scale:** 10000
Report Units: lbf

Applied Force Percent	Series 1 Indicated Reading Ascending	Series 1 Indicated Reading Descending	Series 1 Errors Units Error Asc	Series 1 Errors Percent Error Asc	Series 1 Errors Units Error Desc	Series 1 Errors Percent Error Desc	Series 2 Indicated Reading Ascending	Series 2 Indicated Reading Descending	Series 2 Errors Units Error Asc	Series 2 Errors Percent Error Asc	Series 2 Errors Units Error Desc	Series 2 Errors Percent Error Desc	Repeatability Percent Error Asc	Repeatability Percent Error Desc
0	0.0	0.0	0.00	0.00	0.00	0.00	0.0	0.0	0.00	0.00	0.00	0.00	0.00	0.00
-20	-1997.5		2.50	-0.13			-1997.4		2.60	-0.13			0.00	
-40	-3990.2		9.80	-0.25			-3995.1		4.90	-0.12			0.12	
-60	-5985.7		14.30	-0.24			-5984.9		15.10	-0.25			0.01	
-80	-7989.4		10.60	-0.13			-7993.5		6.50	-0.08			0.05	
-100	-9992.8		7.20	-0.07			-10020.0		20.00	0.20			0.27	

Tension **Range:** 2
Report Units: lbf

Applied Force Percent	Series 1 Indicated Reading Ascending	Series 1 Indicated Reading Descending	Series 1 Errors Units Error Asc	Series 1 Errors Percent Error Asc	Series 1 Errors Units Error Desc	Series 1 Errors Percent Error Desc	Series 2 Indicated Reading Ascending	Series 2 Indicated Reading Descending	Series 2 Errors Units Error Asc	Series 2 Errors Percent Error Asc	Series 2 Errors Units Error Desc	Series 2 Errors Percent Error Desc	Repeatability Percent Error Asc	Repeatability Percent Error Desc
0														
20														
40														
60														
80														
100														

Errors at Zero are computed in % of Range.
The resolution of this Data Set is reflected in the least significant digit reported.
Uncertainty of the data supplied is equal to or less than +/-0.25% of reading for a confidence level of 95%.
This report shall not be reproduced except in full, without the written approval of the laboratory.
Calibrations are performed with standards whose values and measurements are traceable to the National Institute of Standards and Technology.
American Association of Laboratory Accreditation Certificate Number: 1145.01

Out of Tolerance in % column

Notes:

Performed By: Dave Salow Field Service Engineer Date: 30-Mar-05

Signature:

Next Customer Agreed Upon Calibration Date: 30-Mar-06 ACSRep0016

8. REFERENCES

Bentley, C.R., P.W. Pomeroy and H.J. Dorman. 1957. Seismic measurements on the Greenland ice-cap. *Annales de Géophysique*, **13**, 253-285.

Brockamp, B. and P. Pistor. 1969. Ein Beitrag zur seismischen Erforschung der Struktur des groenlaendischen Inlandeises. *Polarforschung*, **37**, 133-146.

Druez, J., C.L. Phan, J.L. Laforte and D.D. Nguyen. 1978-9. The adhesion of glaze and rime on aluminum electrical conductors. *Trans. of the CSME*, **5**(4) 215-220

Druez, J., D.D. Nguyen and Y. Lavoie.1986. Mechanical properties of atmospheric ice. *Cold Regions Science and Technology*, **13**, 67-74

Druez, J., J. Clouthier and L. Claveau. 1987, Etude comparative de la resistance a la traction et a la compression de la glace atmospherique, *Journal de Physique*, **48**(3), C1-337-C1-343

Gammon, P.H., H. Kiefte, et al. 1983. Elastic constants of artificial ice and natural ice samples by brillouin spectroscopy. *J. Glaciology*, **29**(103): 433-460.

Keller, T., U. Motschmann and L. Engelhard. 1999. Modelling the poroelasticity of rocks and ice. *Geophysical Prospecting*, **47**, 509-326.

Shazly, M., Prakash, V. and Lerch, B.A. 2005. High strain rate compression testing of ice (to be published).

Schulson, E.M., P.N. Lim and R.W. Lee. 1984. A brittle-to-ductile transition in ice under tension. *Phil. Mag. A*., **49**, 353-363

Schulson, E.M. 2001. Brittle failure of ice. *Engineering Fracture Mech*., **68**, 1839-1887.

Schulson, E.M., D. Iliescu and A. Fortt. 2005. Characterization of ice for return-to-flight of the space shuttle: Part I: Hard ice. NASA CR-2005-213643/PART1.

Schwartz, J., 2005. Shuttle surface more vulnerable than suspected. New York Times, Jan.20

Shapiro, L.H., J.B. Johnson, M. Sturm and G.L. Blaisdell. 1997. Snow Mechanics: review of the state of knowledge and applications. CRREL Report 97-3, 1- 43.

Thiel, E. and N. Ostenso. 1961. Seismic studies on Antarctic ice shelves. *Geophysics*, **26**, 706-715.

Table 1: The soft ice lots and their characterization.

Ice	Source	Date of arrival at Dartmouth	Specimens (I.D. by sender)	Characterization		
				Microstructure	Density	Strength
15	LM-MAF	11/12/04	1A1-11/10/04	No	No	No
			1A2-11/10/04	No	Yes	No
			1B1-11/10/04	No	Yes	No
			1B2-11/10/04	No	Yes	No
			1B3-11/10/04	Yes	Yes	No
			1C1-11/10/04	Yes	Yes	No
			1D1-11/10/04	No	Yes	No
			1D2-11/10/04	No	Yes	No
			1D3-11/10/04	No	No	No
			1D4-11/10/04	Yes	Yes	No
16	Aerotek-JSC	10/14/04	S1A-10/11/04	Yes	No	No
			S2A-10/11/04	Yes	Yes	No
			S3A-10/11/04	Yes	No	No
			S4A-10/11/04	Yes	Yes	No
			S5A-10/11/04	No	Yes	No
			S1B-10/11/04	Yes	Yes	No
			S2B-10/11/04	Yes	No	No
			S3B-10/11/04	No	Yes	No
17	Aerotek-JSC	11/30/04	CUBE 135	No	No	No
			CUBE 136	No	No	No
			CUBE 137	No	No	No
			CUBE 138	Yes	Yes	No
			CUBE 139	No	No	No
			CUBE 140	No	No	No
			Mfr'd	Yes	Yes	No

Table 1 (continued)

Ice	Source	Date of arrival at Dartmouth	Specimens (I.D. by sender)	Characterization		
				Microstructure	Density	Strength
18	Aerotek-JSC	12/15/04	Cyl. 1 (M fr'd)	No	No	No
			Cyl. 2 (M fr'd)	No	No	No
			Cyl. 3 (M fr'd)	No	No	No
			Cyl. 4 (M fr'd)	No	No	No
			Cyl. 5 (M fr'd)	No	No	No
			Cyl. 6 (M fr'd)	No	No	No
			14-24 (M fr'd)	No	No	No
			14-27	No	No	No
			14-28	No	No	No
			14-30	No	No	No
			14-31	No	No	No
			15-4	No	No	No
			15-4	No	No	No
Snow	Dartmouth IRL	1/24/05 - 2/10/05	Compacted and Sintered			
			• low-degree of packing	Yes	Yes	No
			• medium-degree of packing	Yes	Yes	No
			• high-degree of packing	Yes	Yes	Yes
19	LM-MAF	3/8/05	241-3/5/05	Yes	Yes	No
			2B1-3/5/05	Yes	Yes	No
			2B2-3/5/05	Yes	Yes	No
			2E1-3/5/05	No	Yes	No
			2E2-3/5/05	Yes	Yes	No
20	LM-MAF	3/9/05	2E1-3/7/05	Yes	Yes	Yes
			2E2-3/7/05	Yes	Yes	Yes
			2E3-3/7/05	Yes	Yes	No
			2E4-3/7/05	Yes	Yes	Yes
			2BSTRA1-3/7/05	Yes	Yes	No
			2BSTRA2-3/7/05	Yes	Yes	No
			2BSTRA3-3/7/05	Yes	Yes	Yes
			2BSTRA4-3/7/05	Yes	Yes	No

Table 1 (concluded)

Ice	Source	Date of arrival at Dartmouth	Specimens (I.D. by sender)	Characterization		
				Microstructure	Density	Strength
21	LM-MAF	3/16/05	2D5-3/14/05	Yes	Yes	Yes
			2E1-3/14/05	Yes	Yes	No
			2E2-3/14/05	Yes	Yes	Yes
			2E3-3/14/05	Yes	Yes	Yes
			2E4-3/14/05	Yes	Yes	No
			2E5-3/14/05	Yes	Yes	No
			2BSTRA1-3/14/05	Yes	Yes	No
22	LM-MAF	4/5/05	2E1-3/16/05	Yes	Yes	Yes
			2E2-3/16/05	Yes	Yes	No
			2E3-3/16/05	Yes	Yes	Yes
			2BISTRA1-3/16/05	Yes	Yes	Yes
			2BISTRA2-3/16/05	Yes	Yes	No
25	NASA-JSC	5/19/05	Group A (quick freeze) –4 straight	No	No	No
			Group B (distilled) –3 straight, 1 curved	Yes	No	No
			Group C (normal) –4 straight	No	No	No
			Group D (normal) –3 straight	No	No	No
			Group E (normal) –7 straight	No	No	No
			Group F (normal) –4 straight	No	No	No

Table 2: Density (wet) of Ice-15

LOT	SPECIMEN	WEIGHT IN AIR [grams]	WEIGHT IN n-HEPTANE [grams]	DENSITY [g/cc]
LOT 15	1A2	1.94	0.39	0.890
	1B1	0.45	0.09	0.890
	1B2	2.53	0.44	0.860
	1B3	0.91	0.19	0.900
	1C1	0.75	0.15	0.890
	1D1	1.85	0.40	0.900
	1D2	0.70	0.15	0.900
	1D4	1.24	0.22	0.860

Table 3: Density of Ice-16

LOT	SPECIMEN	WEIGHT IN AIR [grams]	WEIGHT IN n-HEPTANE [grams]	DENSITY [g/cc]
LOT 16	S2-A-10-6-04	2.43	0.46	0.880
	S4-A-10-11-04	3.13	0.61	0.880
	S5-A-10-11-04	3.76	0.67	0.860
	S1-B-10-6-04	2.18	0.46	0.900
		2.36	0.45	0.880
	S3-B-10-6-04	2.44	0.48	0.880

Table 4: Density of Ice-17

Specimen	Dimensions (mm)	Weight (g)	Density [g/cc]
17-138	55.5 x 30.3 x 33.8	41.2	0.730
17-manufactured	75.0 x 46.3 x 49.4	97.9	0.570

Table 5: Density Measurements of Dartmouth Snow Ice Cylinders (01/28/2005)

Specimen / Packing	Length [m]	Mass [g]	Diameter [m]	Density [g/cc]
Low	0.02 0.009	1.13 0.65	0.022 0.022	0.150 0.190
Medium	0.055	6.28	0.022	0.300
High	0.133	28.3	0.022	0.560

Table 6: Dimensions and density (reported by NASA-JSC) on Ice-18

CYL #	Ø (in)	Ø (cm)	LENGTH (in)	LENGTH (cm)	MASS (g)	VOLUME (cm^3)?	DENSITY (g/cc)	DENSITY (lbs/ft^3)	
1	0.8	2.0	1.920	4.88	9.49	15.82	0.600	37.48	Manufactured
2	0.8	2.0	1.950	4.95	9.77	16.06	0.608	37.99	Manufactured
3	0.8	2.0	1.625	4.13	8.50	13.39	0.635	39.66	Manufactured
4	0.8	2.0	1.900	4.83	9.31	15.65	0.595	37.15	Manufactured
5	0.8	2.0	1.950	4.95	9.86	16.06	0.614	38.34	Manufactured
6	0.8	2.0	1.900	4.83	9.78	15.65	0.625	39.03	Manufactured
14-24	0.7	1.8	1.375	3.49	5.72	8.67	0.660	41.20	
14-27	0.7	1.8	1.500	3.81	6.33	9.46	0.669	41.79	
14-28	0.7	1.8	1.375	3.49	6.54	8.67	0.754	47.10	
14-30	0.7	1.8	1.375	3.49	5.83	8.67	0.672	41.99	
14-31	0.7	1.8	1.500	3.81	6.42	9.46	0.679	42.38	
15-4	0.7	1.8	1.375	3.49	5.33	8.67	0.615	38.39	
15-4	0.7	1.8	1.375	3.49	5.33	8.67	0.615	38.39	

Table 7: Density of Ice-19

LOT	SPECIMEN	WEIGHT IN AIR [grams]	WEIGHT IN HEPTANE [grams]	DIMENSIONS OF PRISMS [mm x mm x mm]	DENSITY (by prisms) [g/cc]	DENSITY (by immersion) [g/cc]
LOT 19	3-5-05-2E1	0.49		N/A	N/A	0.883
	3-5-05-2E2	1.83	0.41	N/A	N/A	0.914
	3-5-05-2B1	1.74	0.39	N/A	N/A	0.914
	3-5-05-2B2	0.63	0.13	N/A	N/A	0.894
	3-5-05-241	0.44	0.08	N/A	N/A	0.867

Table 8: Density of Ice-20

LOT	SPECIMEN	WEIGHT IN AIR [grams]	WEIGHT IN HEPTANE [grams]	DIMENSIONS OF PRISMS [mm x mm x mm]	DENSITY (by prisms) [g/cc]	DENSITY (by immersion) [g/cc]
LOT 20	3-7-05-2E1	0.80	0.16	16.69 x 9.37 x 6.53	0.784	0.887
	3-7-05-2E2	0.84	0.17	18.08 x 9.09 x 6.4	0.789	0.890
	3-7-05-2E3	0.86	0.18	14.43 x 8.66 x 7.87	0.874	0.898
	3-7-05-2E4	0.55	0.12	12.63 x 9.55 x 5.33	0.855	0.908
	3-7-05-2BSTRA1	1.21	0.25	N/A	N/A	0.895
	3-7-05-2BSTRA2	1.89	0.4	N/A	N/A	0.900
	3-7-05-2BSTRA3	0.70	0.15	16.36 x 10.49 x 4.90	0.832	0.903
	3-7-05-2BSTRA4	1.21	0.25	12.52 x 11.76 x 9.83	0.836	0.895

Table 9: Density of Ice-21

LOT	SPECIMEN	WEIGHT IN AIR [grams]	WEIGHT IN HEPTANE [grams]	DIMENSIONS OF PRISMS [mm x mm x mm]	DENSITY (by prisms) [g/cc]
LOT 21	3-14-05-2E1	0.94	N/A	13.34 x 10.95 x 8.28	0.778
	3-14-05-2E2	0.86	N/A	11.76 x 8.99 x 9.30	0.875
	3-14-05-2E3	0.89	N/A	13.61 x 9.73 x 7.72	0.870
	3-14-05-2E4	0.30	N/A	13.49 x 5.59 x 4.78	0.834
	3-14-05-2E5	0.35	N/A	13.74 x 7.54 x 3.99	0.847
	3-14-05-2D5	0.60	N/A	14.96 x 7.37 x 7.01	0.777
	3-14-05-2BSTRA1	0.69	N/A	14.43 x 9.63 x 6.35	0.782

Table 10: Density of Ice-22

LOT	SPECIMEN	WEIGHT IN AIR [grams]	WEIGHT IN HEPTANE [grams]	DIMENSIONS OF PRISMS [mm x mm x mm]	DENSITY (by prisms) [g/cc]
LOT 22	3-16-05-2E1	0.410	N/A	10.82 x 7.49 x 5.82	0.869
		0.209	N/A	9.40 x 5.97 x 5.11	0.730
	3-16-05-2E2	0.687	N/A	12.43 x 8.53 x 7.34	0.882
		0.445	N/A	11.46 x 6.76 x 6.52	0.882
	3-16-05-2E3	1.043	N/A	16.71 x 9.21 x 7.65	0.887
		0.629	N/A	9.65 x 9.14 x 8.03	0.888
	3-16-05-2BSTRA1	0.757	N/A	16.03 x 8.18 x 6.78	0.853
	3-16-05-2BSTRA2	0.136	N/A	8.86 x 4.69 x 4.22	0.776

Table 11: Compressive strength of Ice-20, Ice-21 and Ice-22 at -10 °C at 0.3 s^{-1}

LOT	SPECIMEN	TEST	DIMENSIONS OF PRISMS			DENSITY (by prisms) [g/cc]	STRAIN RATE [s^{-1}]	STRENGTH [MPa]
			X1 [mm]	X2 [mm]	H [mm]			
LOT 20	3-7-05-2E1	C-91	9.37	6.53	16.69	0.784	0.24	3.2
	3-7-05-2E2	C-119	9.09	6.4	18.08	0.789	0.27	2.7
	3-7-05-2E3	C-93	8.66	7.87	14.43	0.874		(X)
	3-7-05-2E4	C-121	9.55	5.33	12.63	0.855	0.26	3.1
	3-7-05-2BSTRA1		N/A	N/A	N/A	N/A		
	3-7-05-2BSTRA2		N/A	N/A	N/A	N/A		
	3-7-05-2BSTRA3	C-120	10.49	4.90	16.36	0.832	0.28	1.8
	3-7-05-2BSTRA4	C-92	11.76	9.83	12.52	0.836		(X)
LOT 21	3-14-05-2E1	C-88	10.95	8.28	13.34	0.778		(X)
	3-14-05-2E2	C-87	9.30	8.99	11.76	0.875	0.33	3.1
	3-14-05-2E3	C-89	9.73	7.72	13.61	0.870	0.33	3.4
	3-14-05-2E4		5.59	4.78	13.49	0.834		(TS)
	3-14-05-2E5	C-90	7.54	3.99	13.74	0.847		(X)
	3-14-05-2D5	C-86	7.37	7.01	14.96	0.777	0.28	3.9
	3-14-05-2BSTRA1		9.63	6.35	14.43	0.782		(TS)
LOT 22	3-16-05-2E1	C-118	7.49	5.82	10.82	0.869	0.28	4.0
	3-16-05-2E2	C-116	12.43	8.53	7.34	0.882		(X)
		C-117	11.46	6.76	6.52	0.882		(X)
	3-16-05-2E3	C-113	16.71	9.21	7.65	0.887	0.27	5.4
		C-114	9.65	9.14	8.03	0.888		(X)
	3-16-05-2BSTRA1	C-115	16.03	8.18	6.78	0.853	0.29	6.3
	3-16-05-2BSTRA2		8.86	4.69	4.22	0.776		(TS)

(X) - Specimen damaged while loaded. No tests were performed on such specimens.
(TS) – Prismatic specimen *too small* to be tested. Only used for density measurements.

Table 12: Compressive strength of 3-5 day compacted IRL snow ice at -10 °C at ~0.3 s^{-1}.

Specimen (Test #)	Length [mm]	Diameter [mm]	Mass [g]	Density [g/cc]	Measured strain rate [1/s]	Failure stress [MPa]
C-74	65	22.1	N/A	N/A	0.27	1.7
C-75	60.7	22.1	N/A	N/A	0.25	1.9
C-76	66.2	22.1	N/A	N/A	0.26	1.5
C-77	63.7	22.1	N/A	N/A	0.26	1.6
C-78	64.3	22.1	14.48	0.587	0.35	2.1
C-79	64.4	22.1	14.49	0.587	N/A	N/A*
C-80	64.3	22.1	14.87	0.600	0.47	2.3
C-81	64.3	22.1	14.97	0.600	.93	2.4
C-82	64.2	22.1	14.80	0.600	N/A	N/A*
C-83	62.7	22.1	14.31	0.595	0.8	1.6**
C-84	64.3	22.1	14.32	0.580	0.37	1.4
C-85	64.3	22.1	15.32	0.620	0.097	2.5

(*) Data acquisition system did not collect data.

(**) Actual failure stress could be higher. Due to the limited scanning rate of the data acquisition system used in these tests(1000 scans/sec) it is possible that the peak of the stress-time curve for this high strain rate test curve was missed (it occurred between two consecutive scans). Previous test (C-81) performed at the highest strain rate had 3 data points per loading ramp. In comparison test C-83 had only two.

Table 13: Comparison of the compressive strength of different lots of soft ice deformed at -10 °C at ~0.3 s^{-1}

Material / Characteristics	Compacted Snow Ice	Ice-20	Ice-21	Ice-22
Density-dry , (g/cc)	0.560	0.828 ± 0.036	0.823 ± 0.044	0.846 ± 0.060
Grain size (mm)	~0.06	~0.1 - 5	~0.3 - 10	~0.3 - 10
Compressive strength (MPa)	1.9 ± 0.3	2.7 ± 0.7	3.5 ± 0.4	5.2 ± 1.2

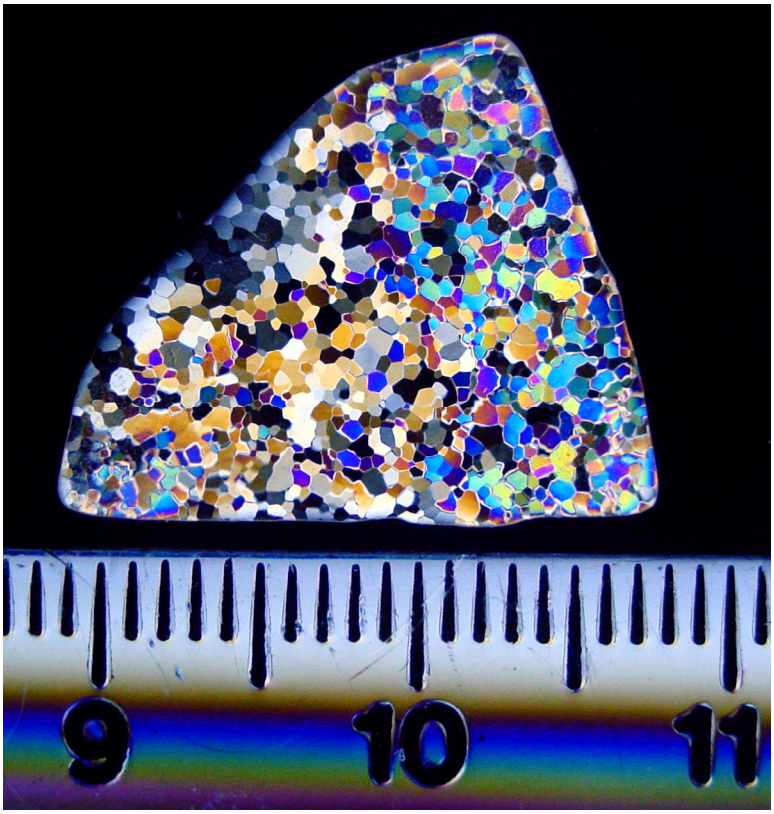

Figure 1: Ice-15, microstructure of specimen 1B3.

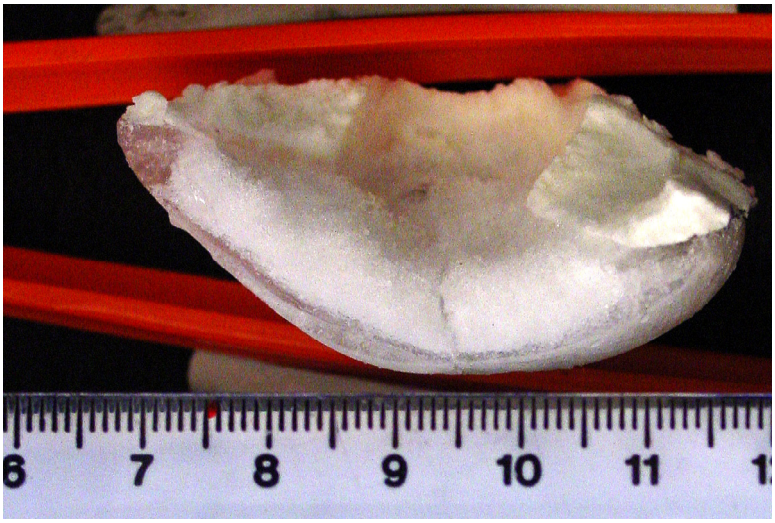

a)

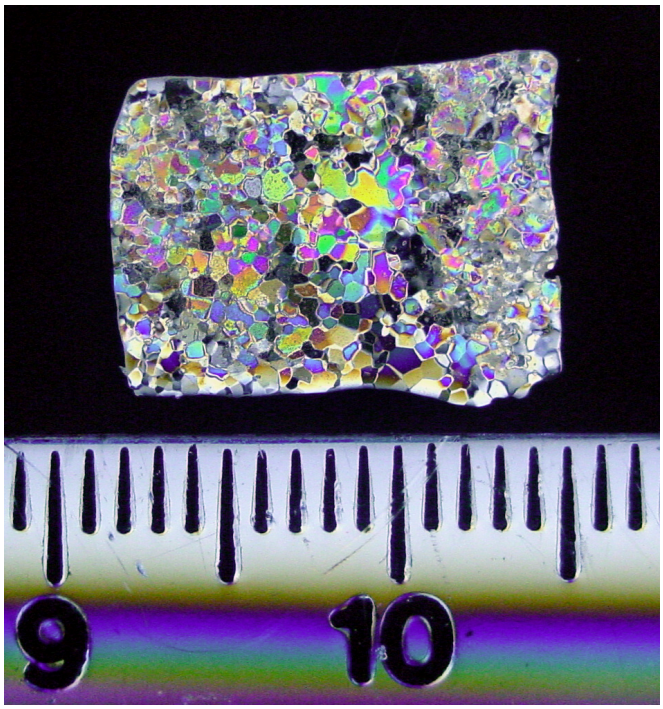

b)

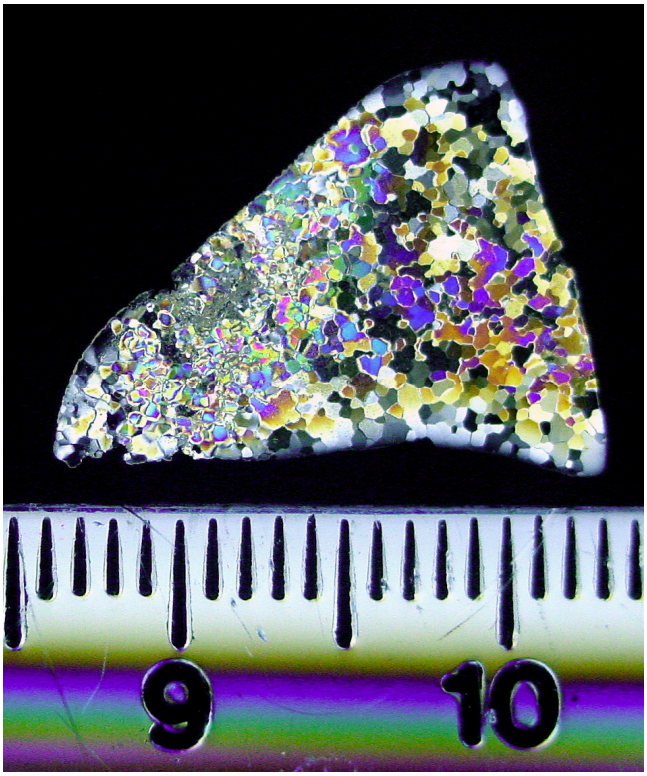

c)

Figure 2: Ice 15, specimen 1C1:
a) composite of frost-like ice (white) and cloudy ice;
b) microstructure of the cloudy ice;
c) another view of the microstructure of the cloudy ice.

a)

b)

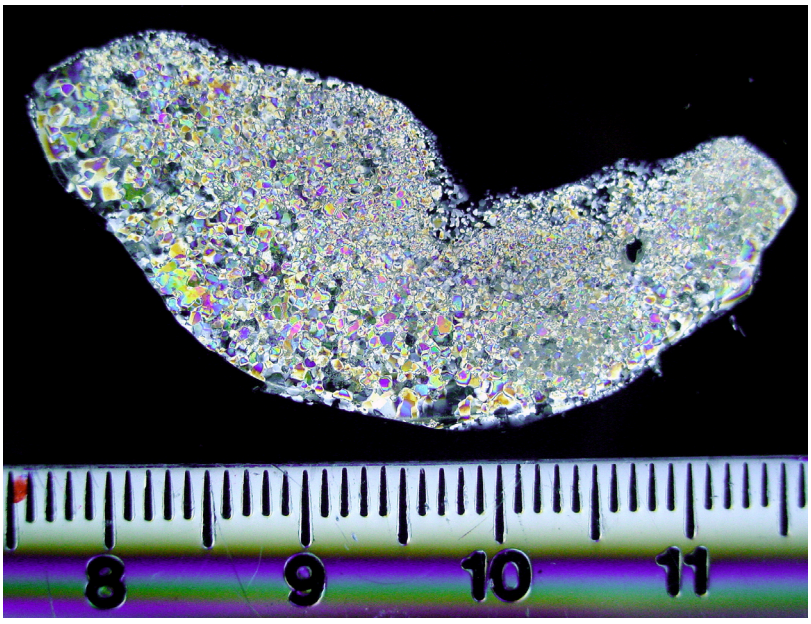

c)

Figure 3: Ice-15, specimen 1D4:
a) frost-ice composite on foam insulation;
b) section through ice layer of composite;
c) microstructure of the ice.

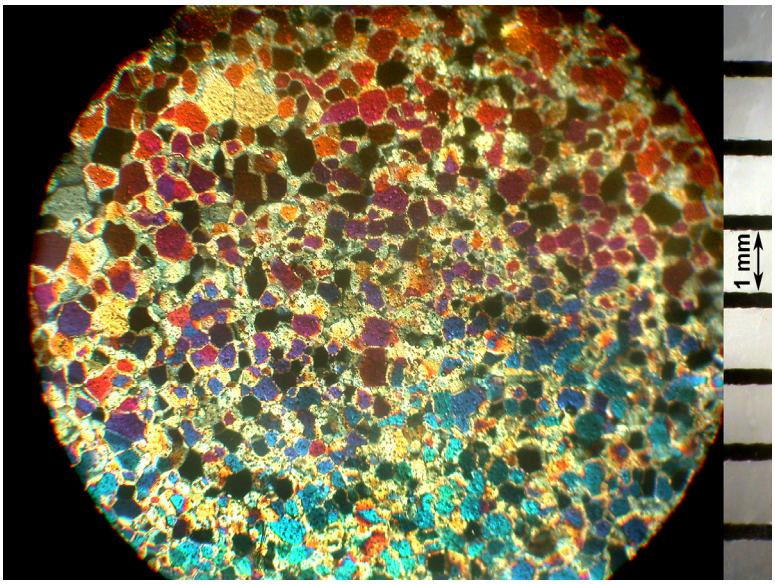

a)

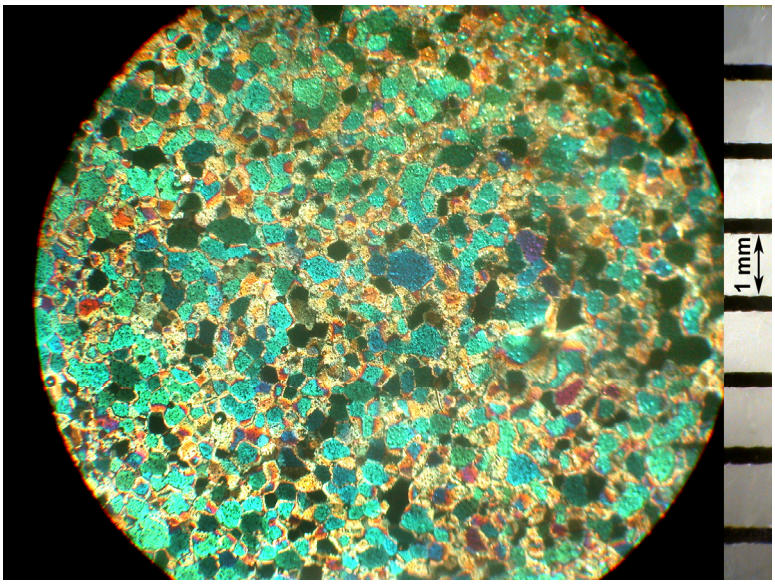

b)

Figure 4: Ice-16, specimen S1-A-10/11/04:
a) microstructure in section parallel to cold plate;
b) another view of microstructure parallel to cold plate.

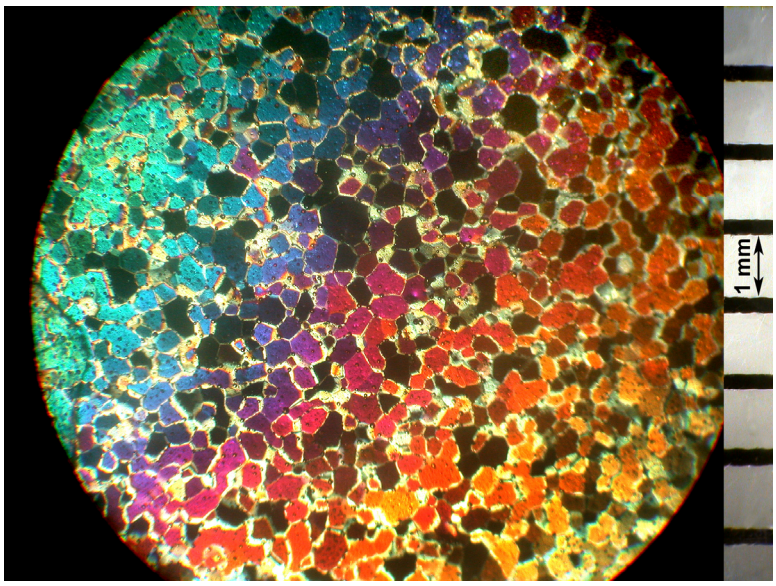

Figure 5: Ice-16, specimen S2-A-10/6/04, microstructure parallel to cold plate.

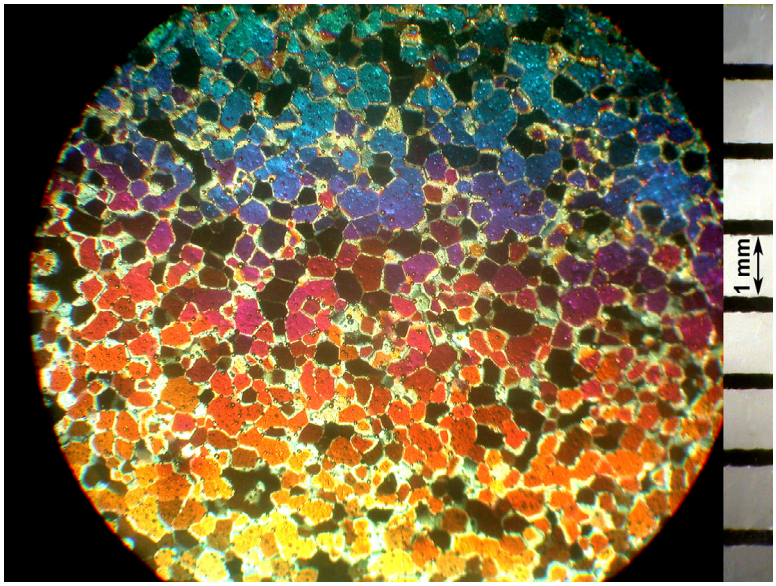

Figure 6: Ice-16, specimen S3-A-10/11/04, microstructure parallel to cold plate.

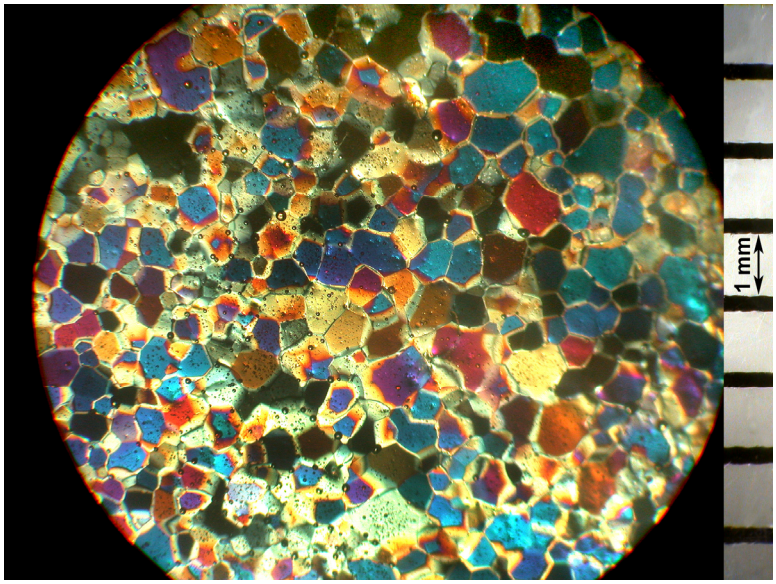

Figure 7: Ice-16, specimen S1-B-10/6/04, microstructure parallel to cold plate.

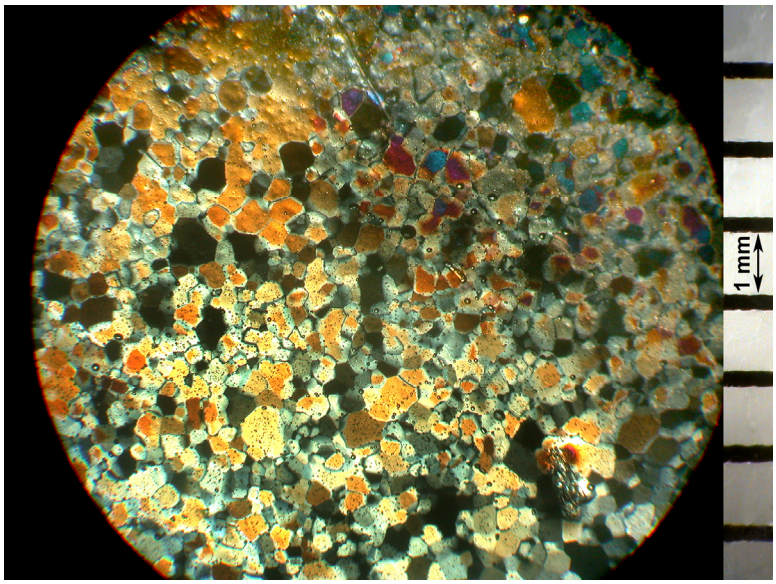

a)

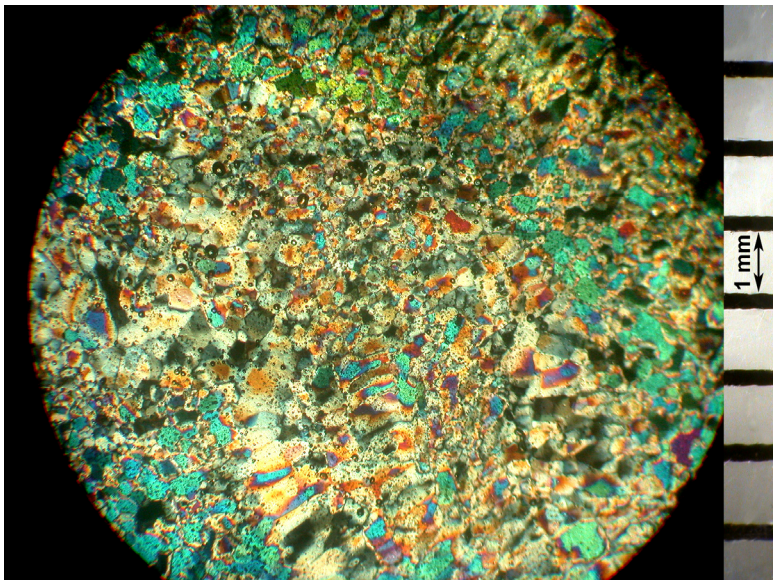

b)

Figure 8: Ice-16, specimen S2-B-10/6/04:
a) microstructure parallel to cold plate;
b) another view of microstructure parallel to cold plate.

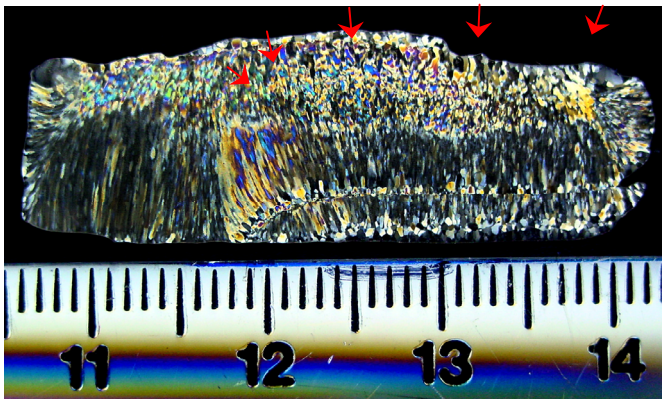

a)

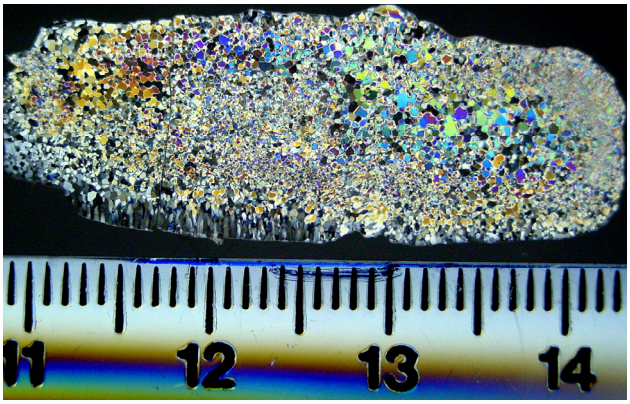

b)

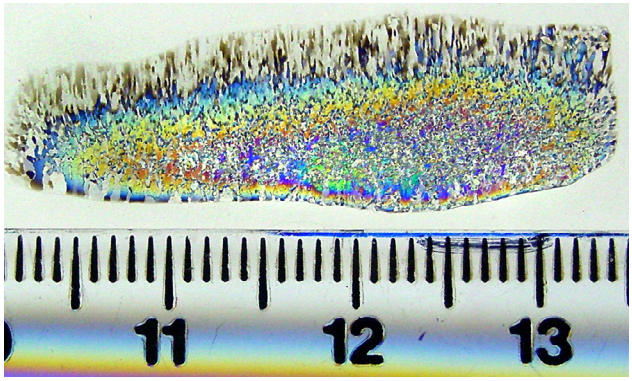

c)

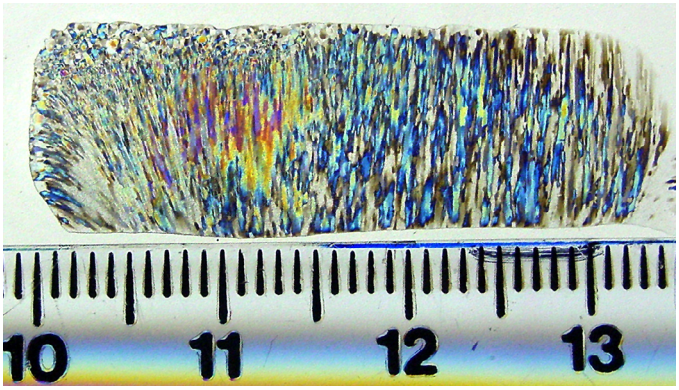

d)

Figure 9: Ice-16, specimen S4-A-10/11/04:
a) microstructure in section perpendicular to cold plate;
b) microstructure in another perpendicular section;
c) microstructure in still another perpendicular section;
d) microstructure in 4th perpendicular section.

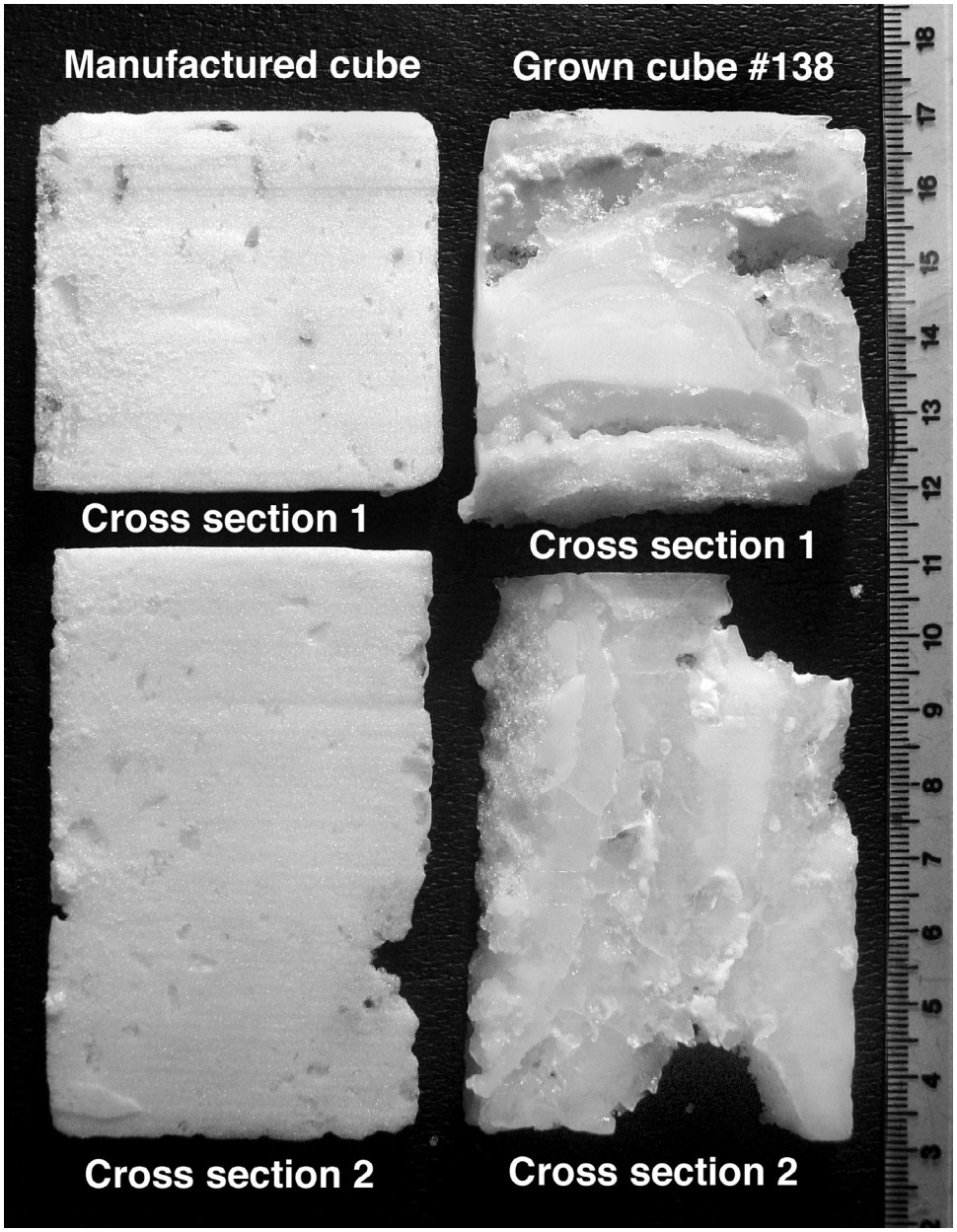

Figure 10: Ice-17, macroscopic views of specimen 17-138 (frost and sprayed) and of manufactured specimen.

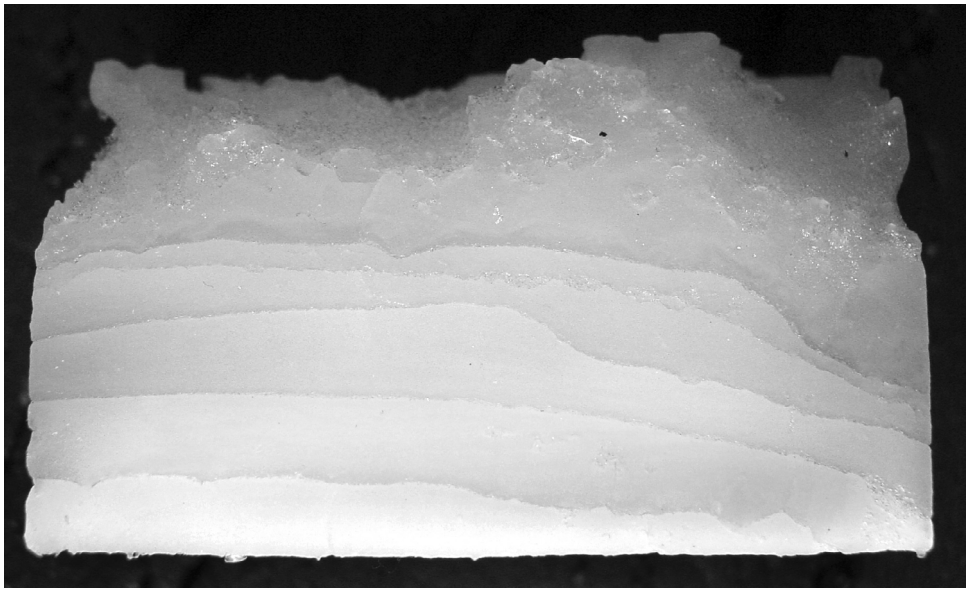

Figure 11: Ice-17, specimen 17-138, macroscopic view showing layers (scale: length = 55.4 mm).

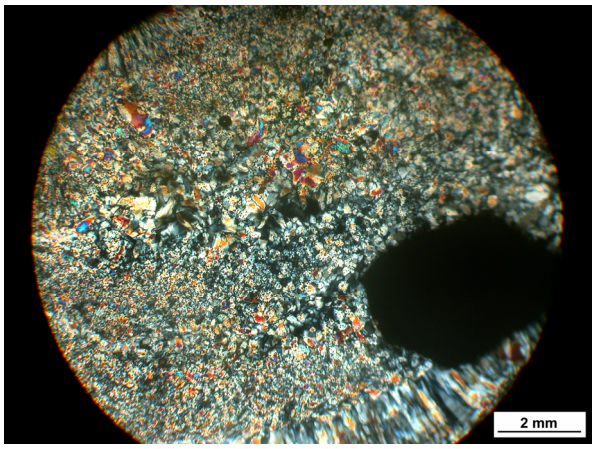

a)

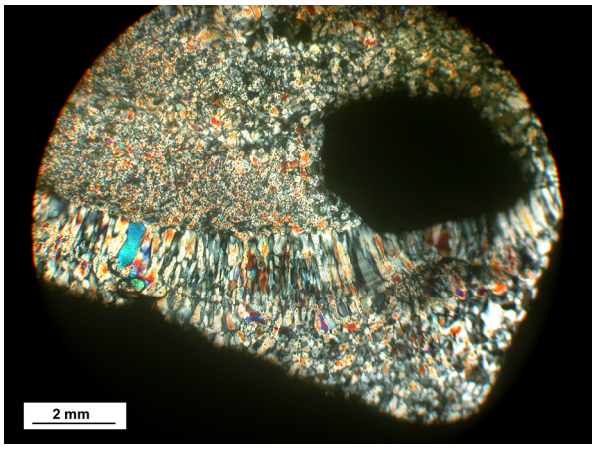

b)

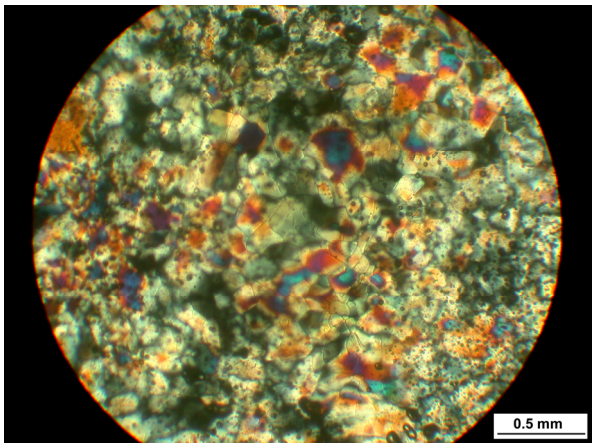

c)

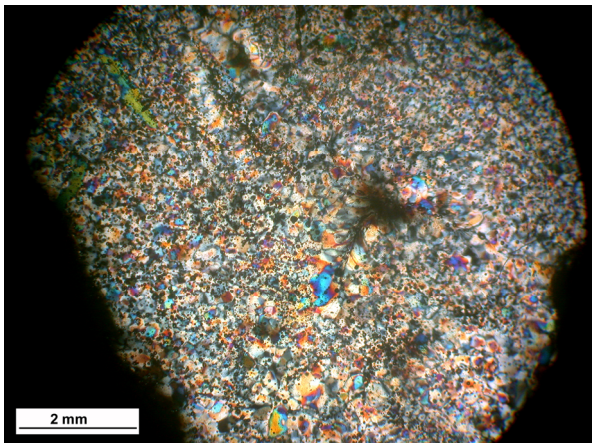

d)

Figure 12: Ice-17, specimen 17-138:
a) microstructure;
b) another view of microstructure;
c) magnified view of microstructure in b);
d) microstructure in section perpendicular to that of a), b), c).

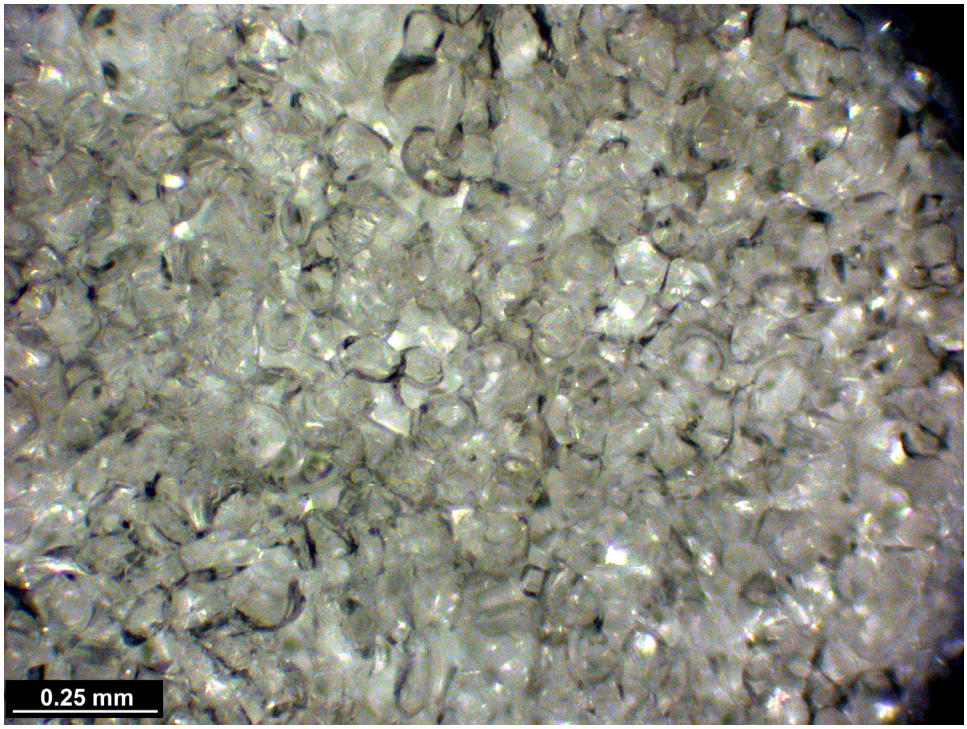

Figure 13: Ice 17, microstructure of manufactured specimen.

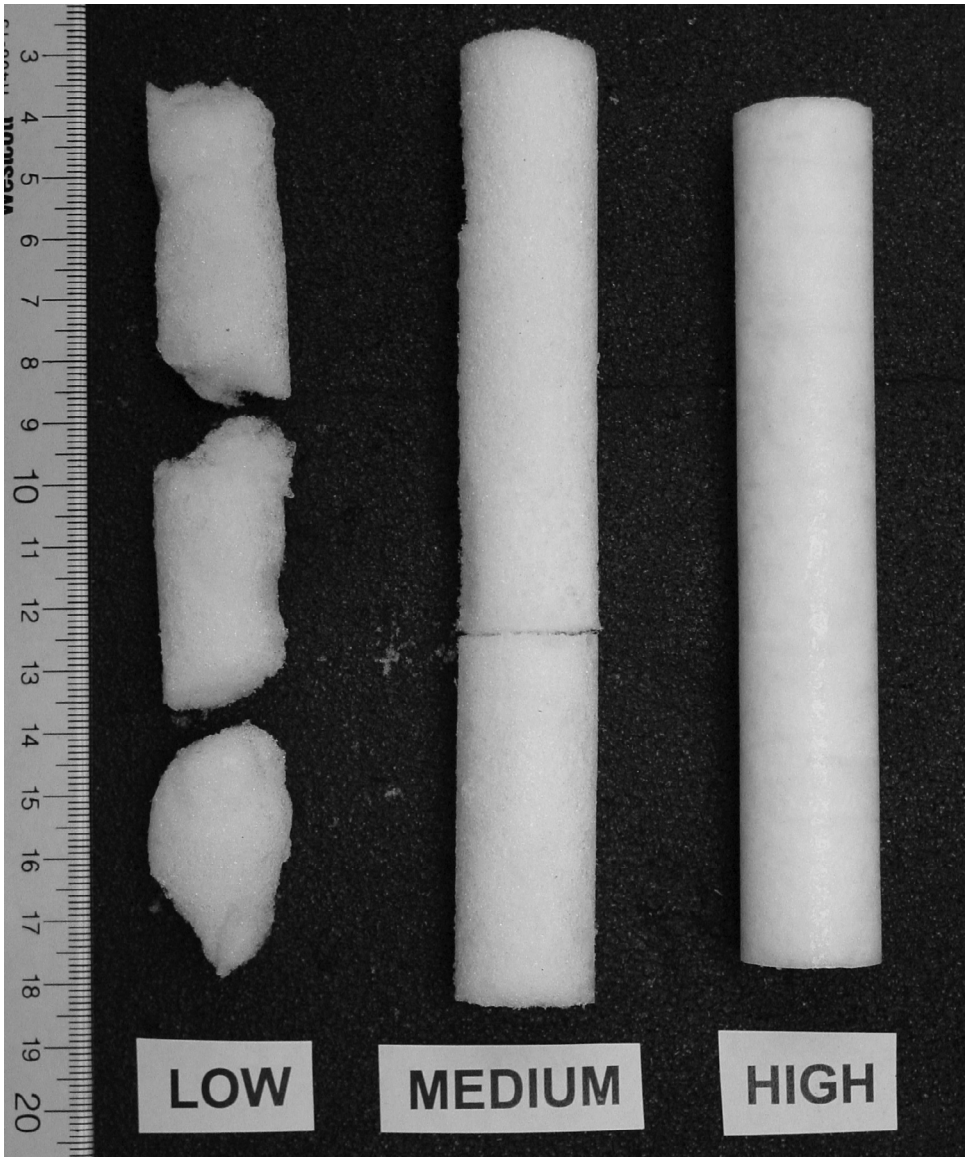

Figure 14: Snow ice cylinders from Ice Research Lab (IRL) after 3-day sintering at -10 °C following low, medium and high degree of consolidation by packing.

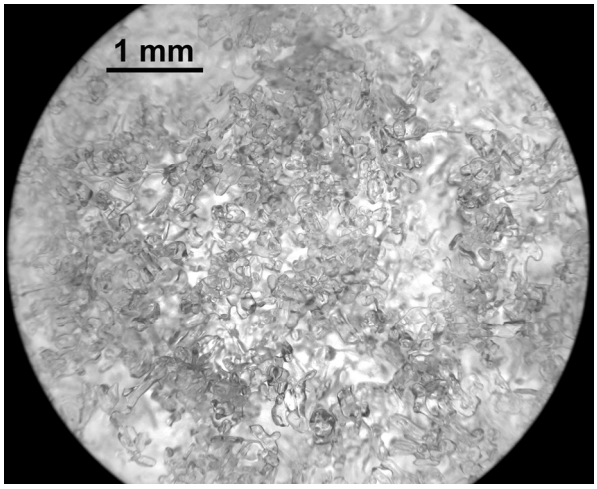

a)

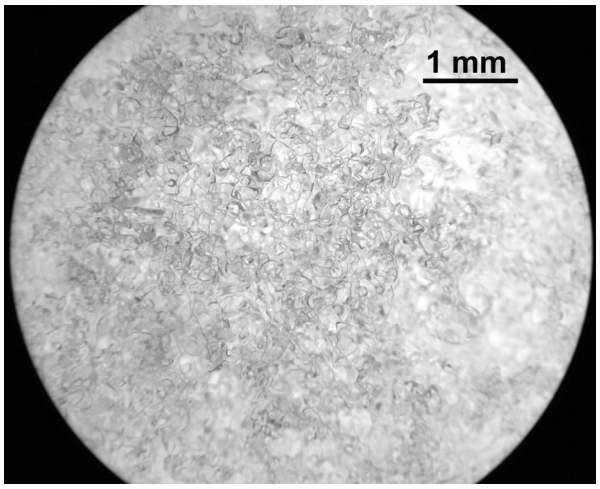

b)

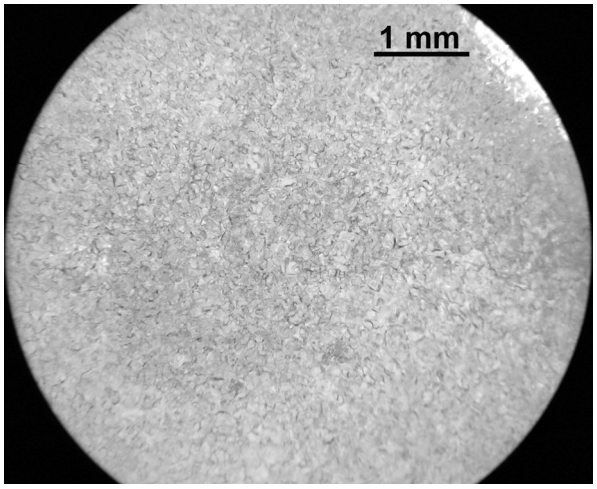

c)

Figure 15: IRL snow ice, showing microstructure of specimens shown in Figure 14:
a) low packing;
b) medium packing;
c) high packing.

a)

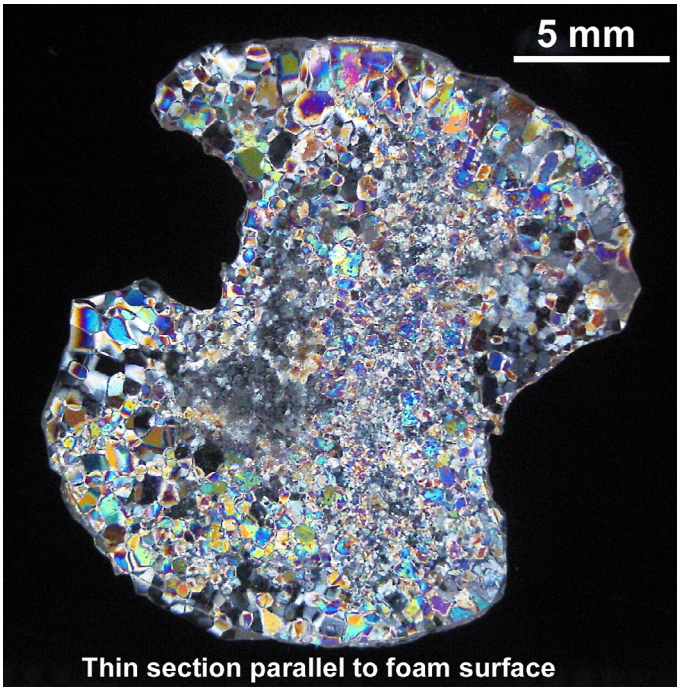

b)

Figure 16: Ice-19, specimen 241-3/5/05:
a) macroscopic view;
b) microstructure.

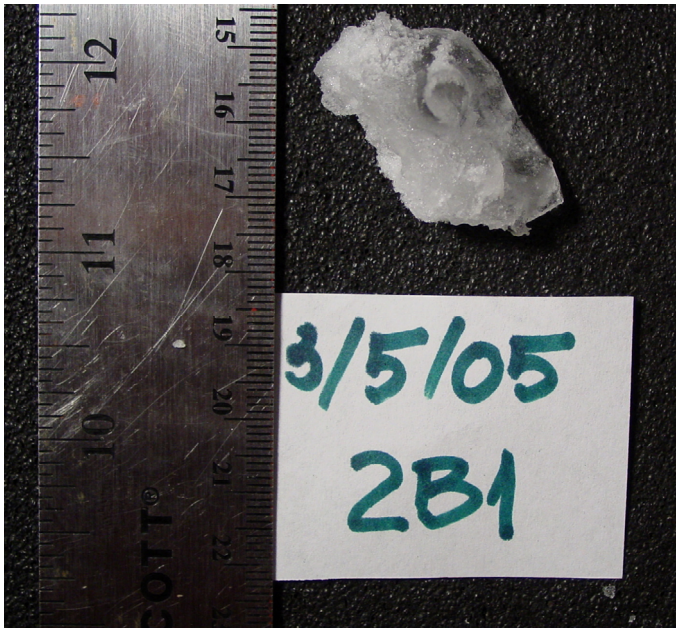

a)

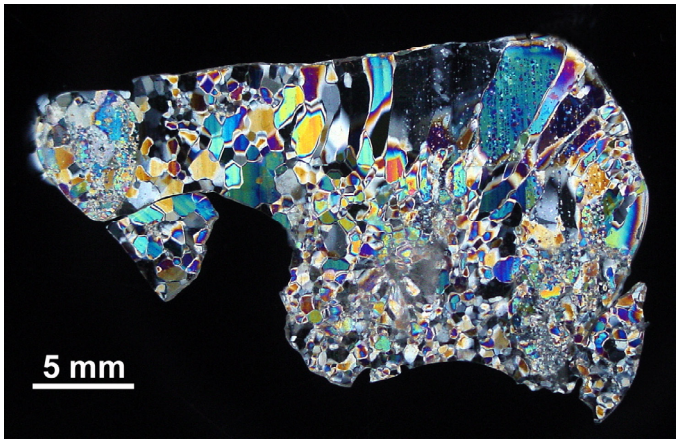

b)

Figure 17: Ice-19, specimen 2B1-3/5/05:
a) macroscopic view;
b) microstructure.

a)

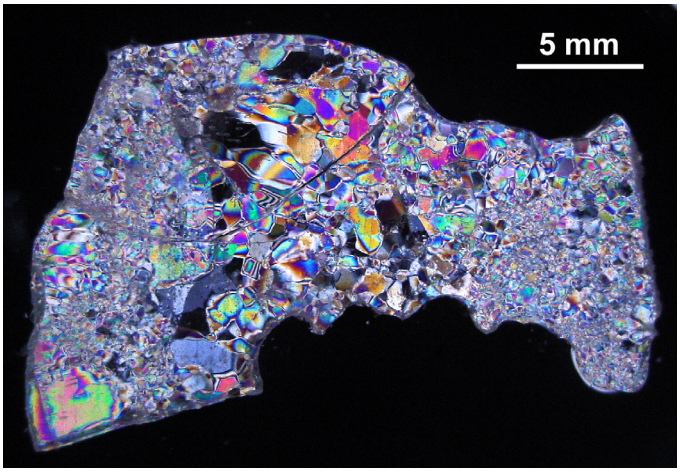

b)

Figure 18: Ice-19, specimen 2B2-3/5/05:
a) macroscopic view;
b) microstructure.

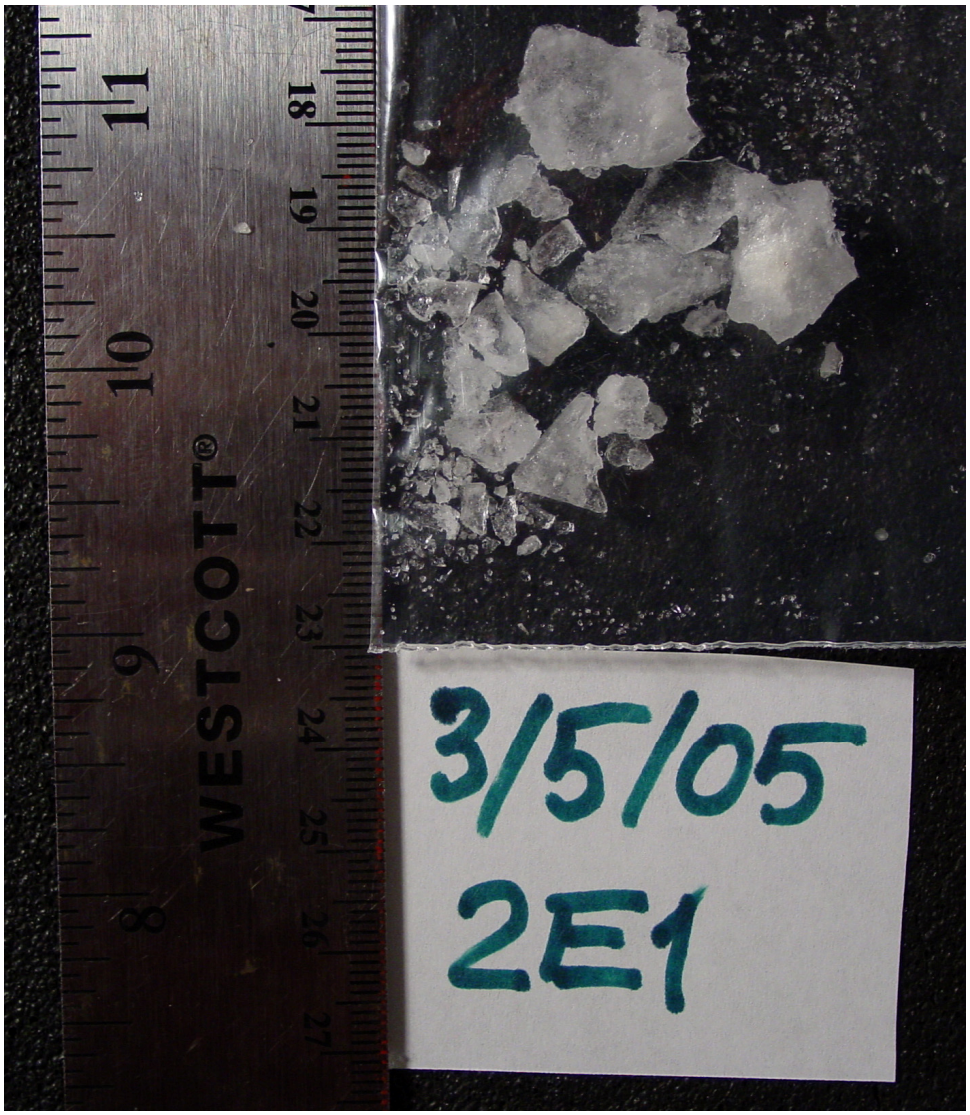

Figure 19: Ice-19, specimen 2E1-3/5/05

a)

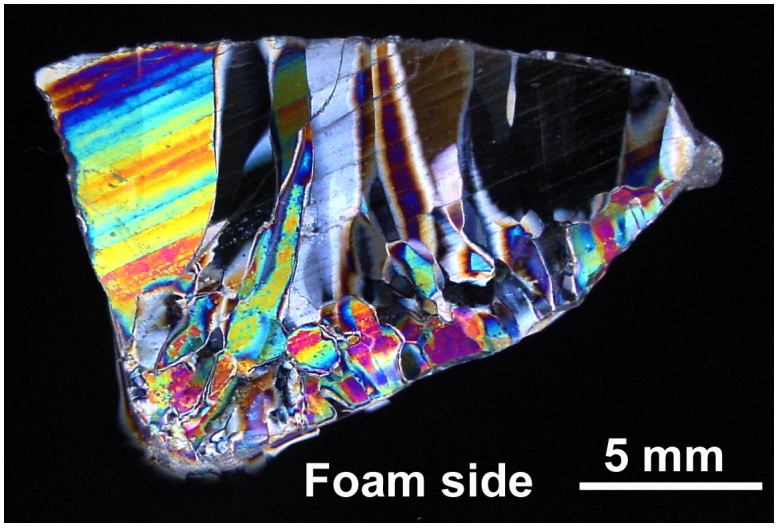

b)

Figure 20: Ice-19, specimen 2E2-3/5/05:
a) macroscopic view;
b) microstructure.

a)

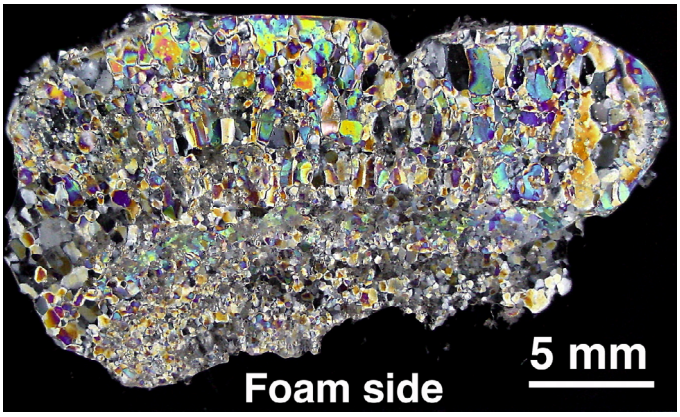

b)

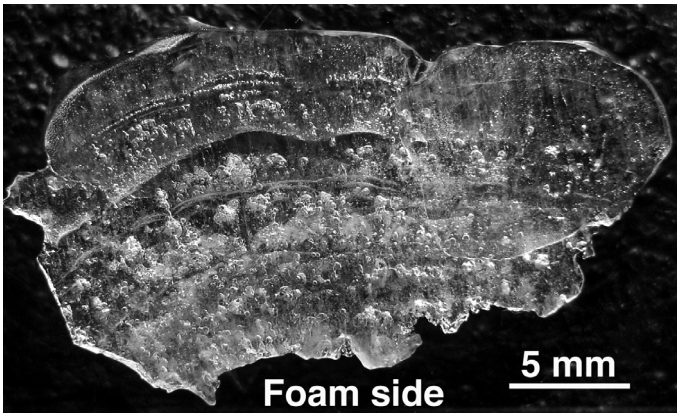

c)

Figure 21: Ice-20, specimen 2E1-3/7/05:
a) macroscopic view;
b) microstructure, polarized;
c) microstructure, direct light.

a)

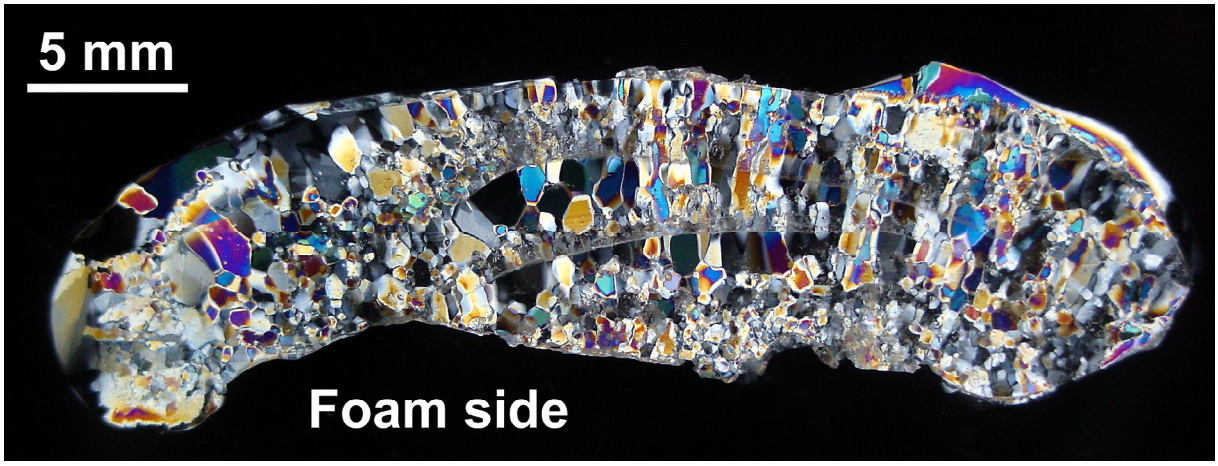

b)

Figure 22: Ice-20, specimen 2E2-3/7/05:
a) macroscopic view;
b) microstructure.

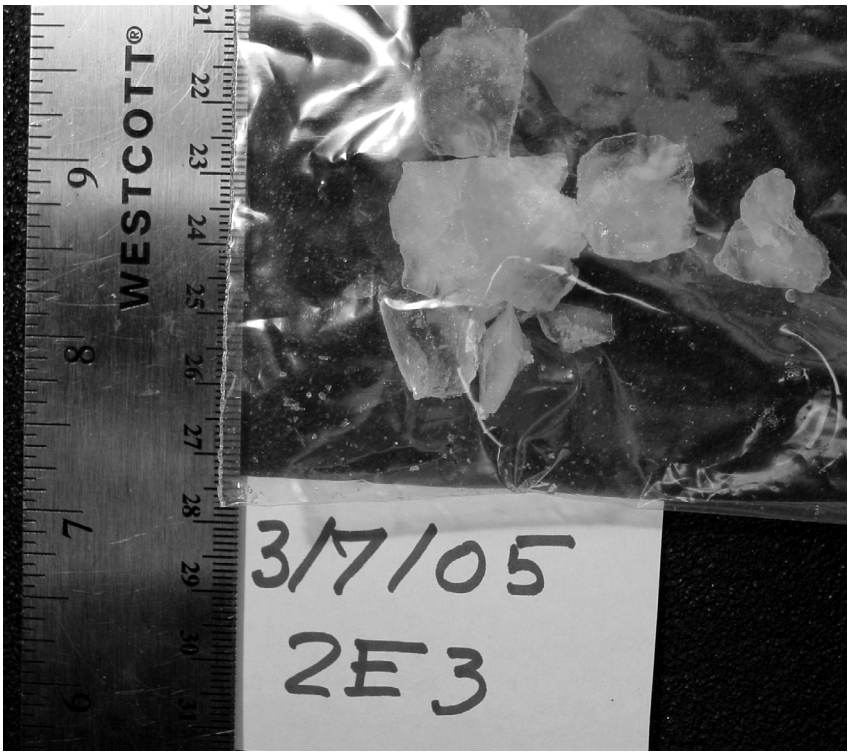

a)

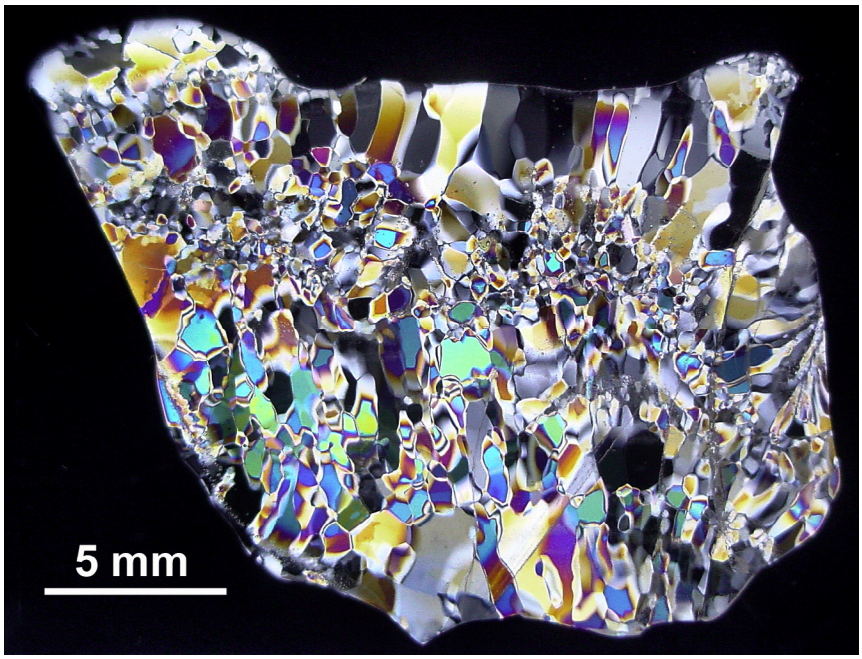

b)

Figure 23: Ice-20, specimen 2E3-3/7/05:
a) macroscopic view;
b) microstructure.

a)

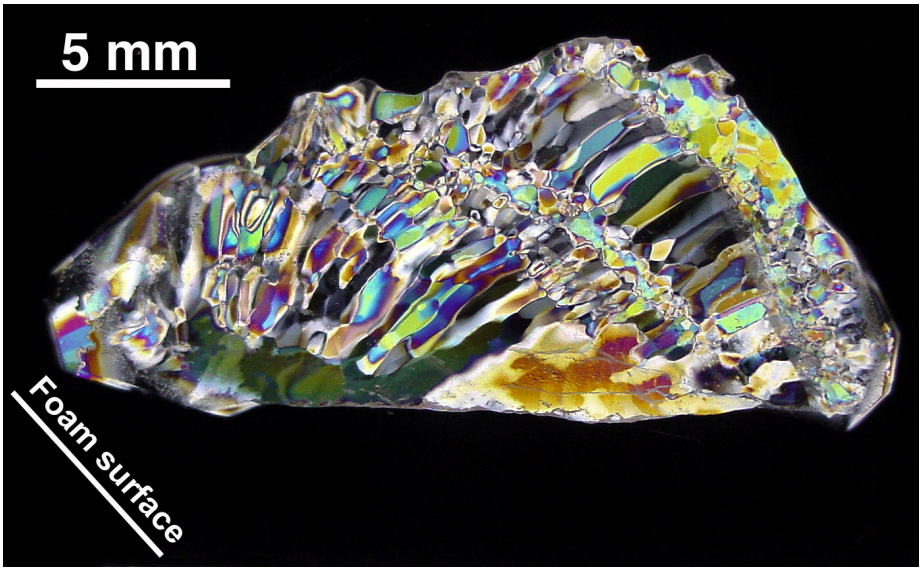

b)

Figure 24: Ice-20, specimen 2E4-3/7/05:
a) macroscopic view;
b) microstructure.

a)

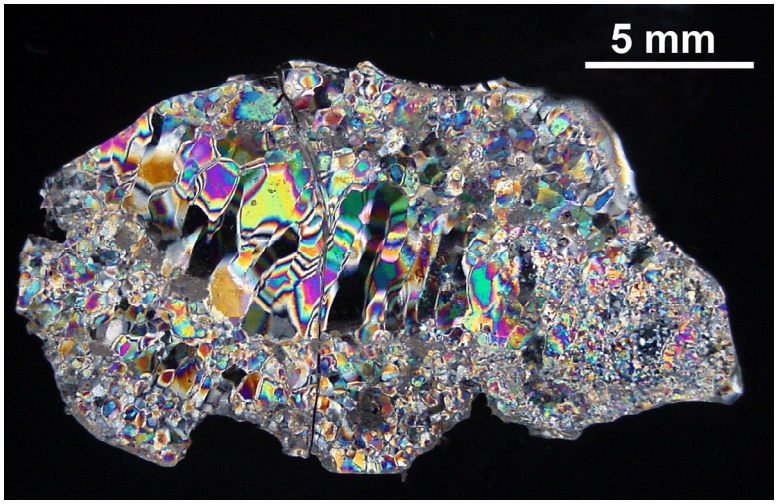

b)

Figure 25: Ice-20, specimen 2BSTRA1-3/7/05:
a) macroscopic view;
b) microstructure.

a)

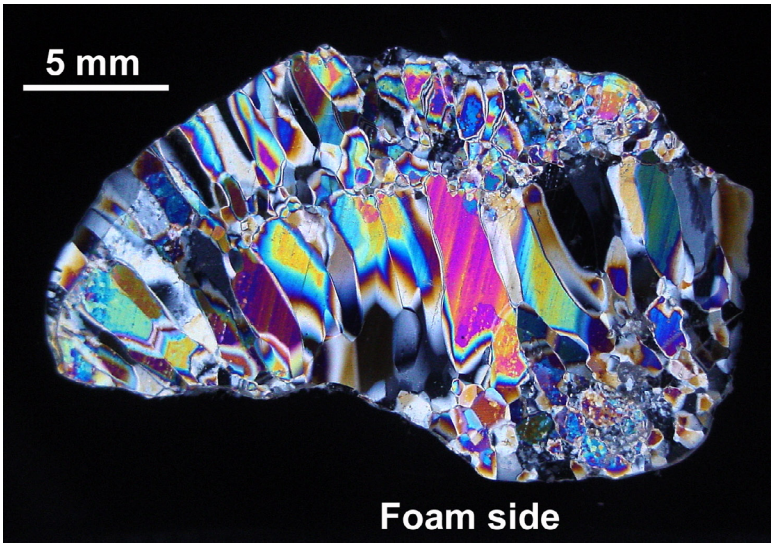

b)

Figure 26: Ice-20, specimen 2BSTRA2-3/7/05:
a) macroscopic view;
b) microstructure.

a)

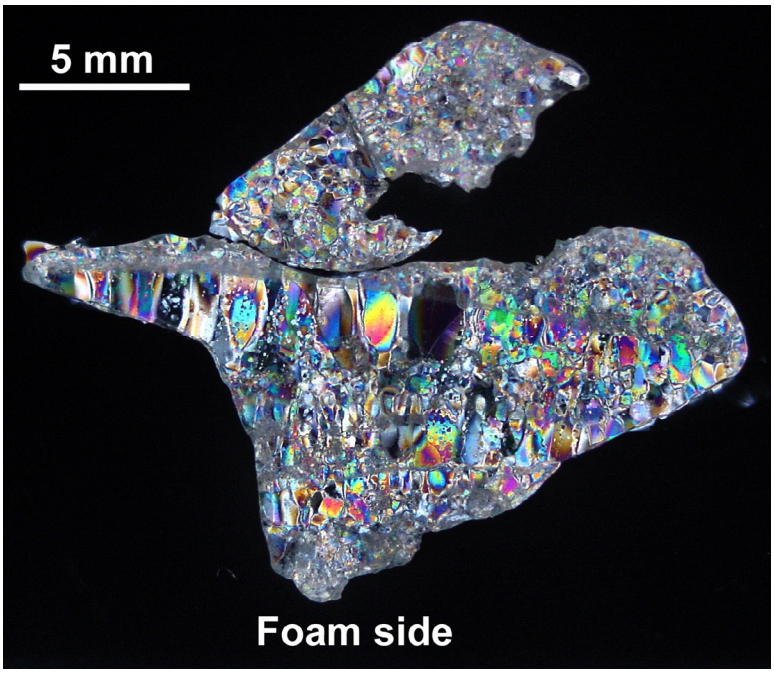

b)

Figure 27: Ice-20, specimen 2BSTRA3-3/7/05:
a) macroscopic view;
b) microstructure.

a)

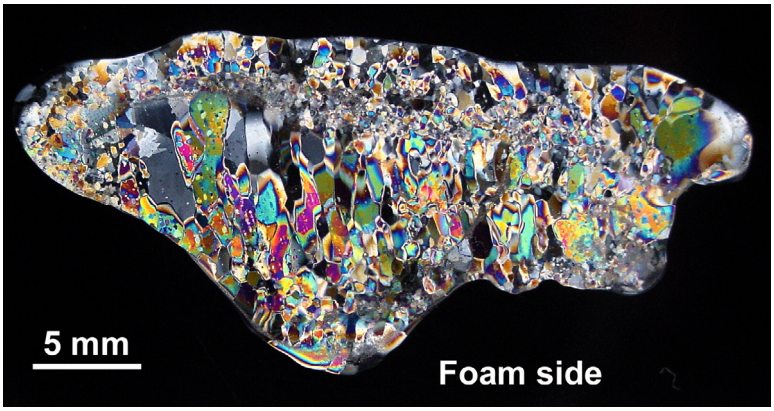

b)

Figure 28: Ice-20, specimen 2BSTRA4-3/7/05:
a) macroscopic view;
b) microstructure.

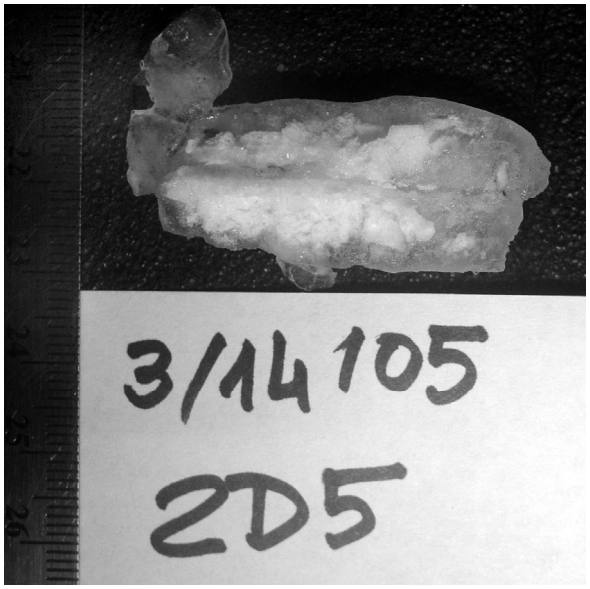

a)

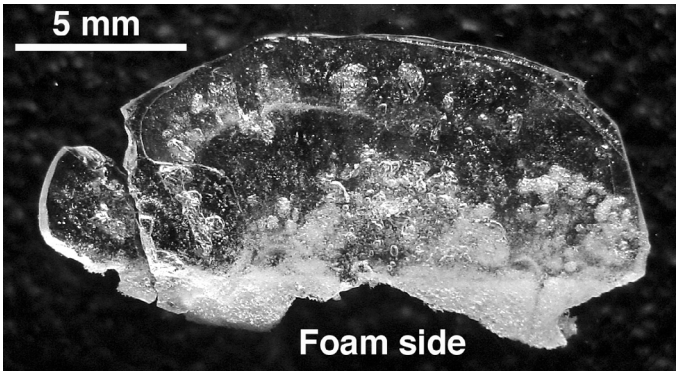

b)

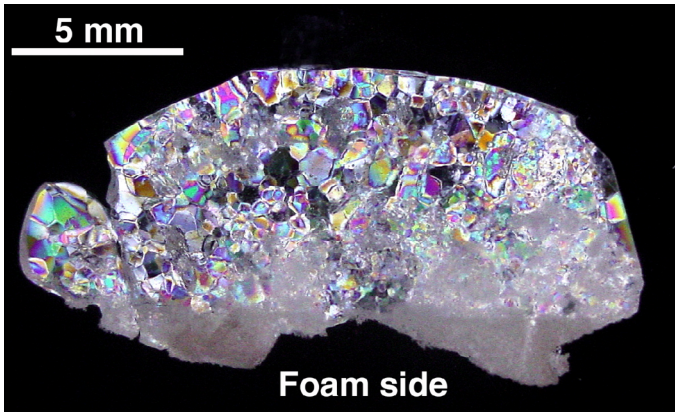

c)

Figure 29: Ice-21, specimen 2D5-3/14/05:
a) macroscopic view;
b) microstructure, direct light;
c) microstructure, polarized.

a)

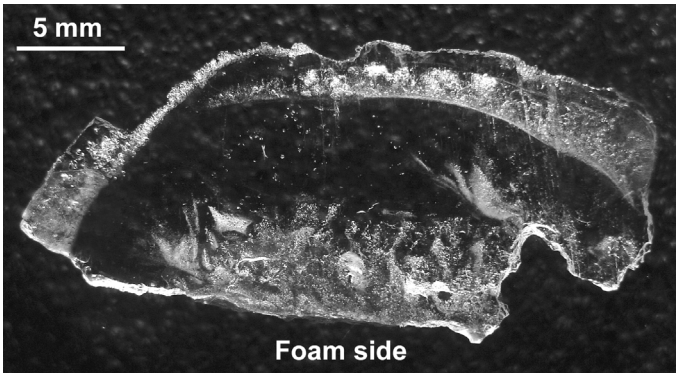

b)

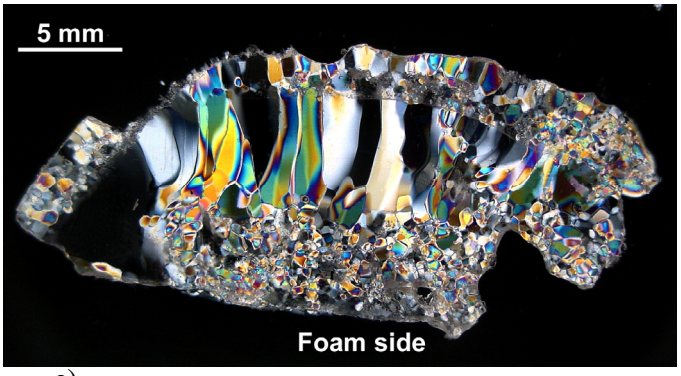

c)

Figure 30: Ice-21, specimen 2E1-3/14/05:
a) macroscopic view;
b) microstructure, direct light;
c) microstructure, polarized.

a)

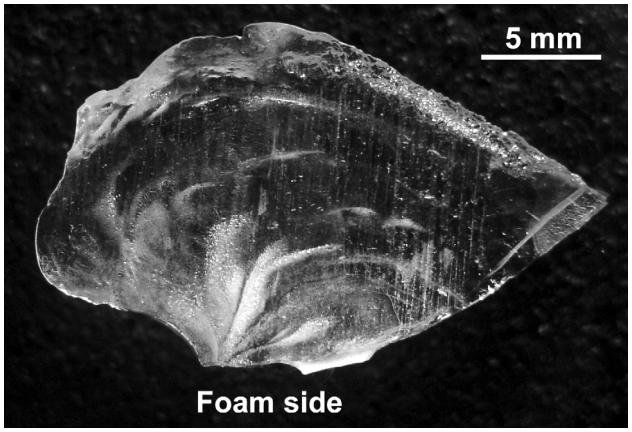

b)

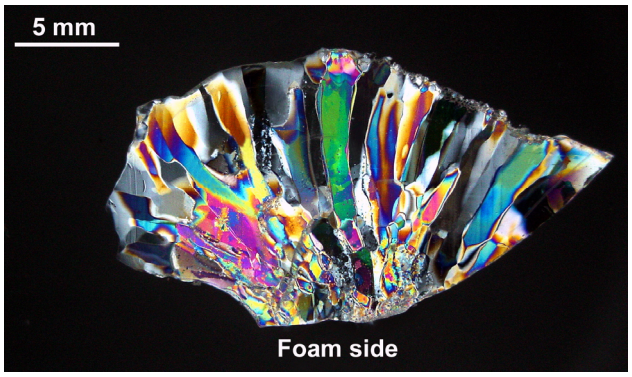

c)

Figure 31: Ice-21. specimen 2E2-3/14/05:
a) macroscopic view;
b) microstructure, direct light;
c) microstructure, polarized.

a)

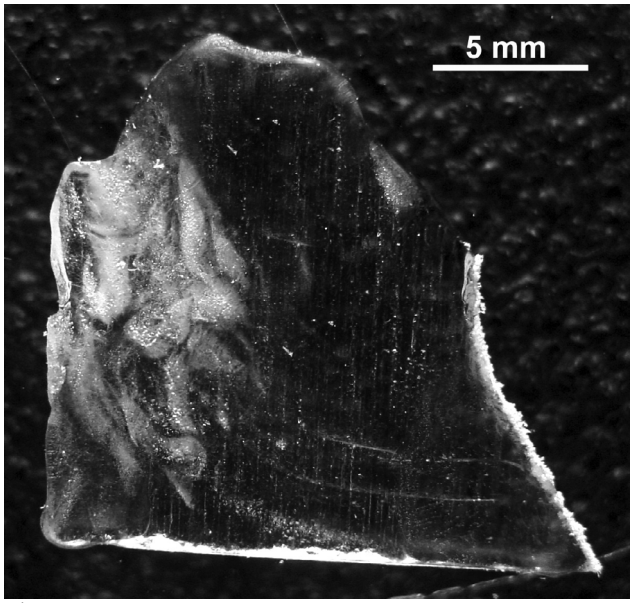

b)

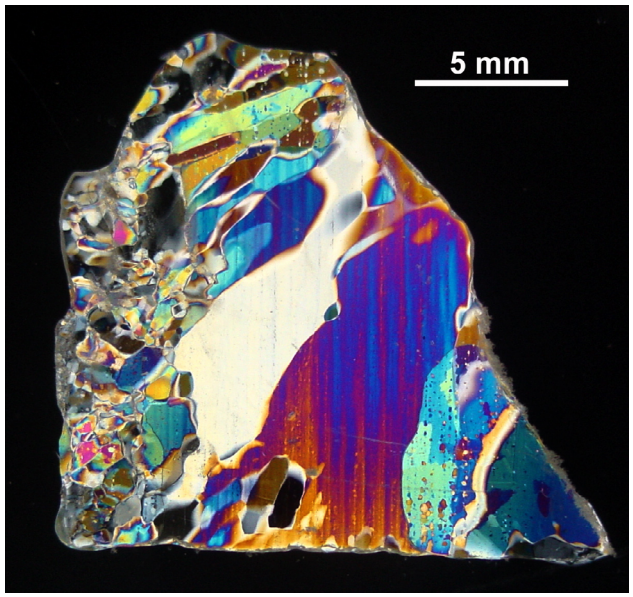

c)

Figure 32: Ice-21, specimen 2E3-3/14/05:
a) macroscopic view;
b) microstructure, direct light;
c) microstructure, polarized.

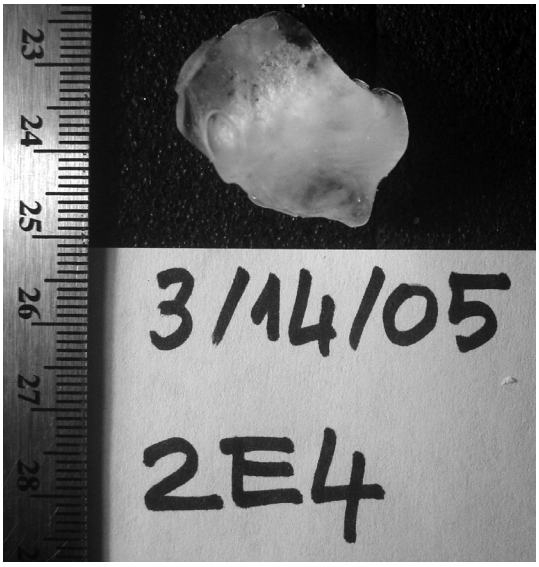

a)

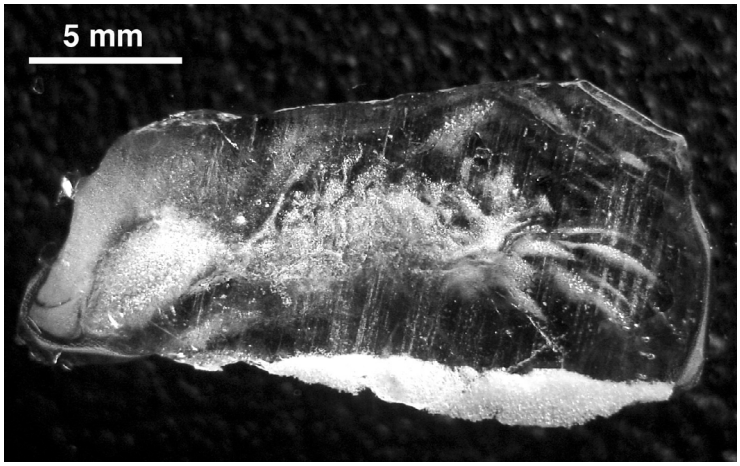

b)

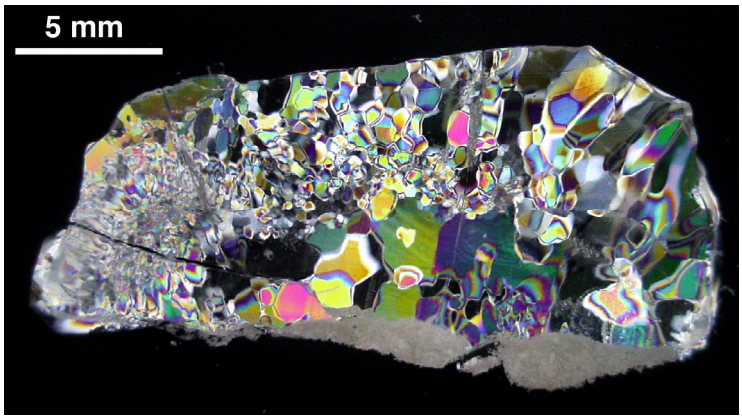

c)

Figure 33: Ice-21, specimen 2E4-3/14/05:
a) macroscopic view;
b) microstructure, direct light;
c) microstructure, polarized.

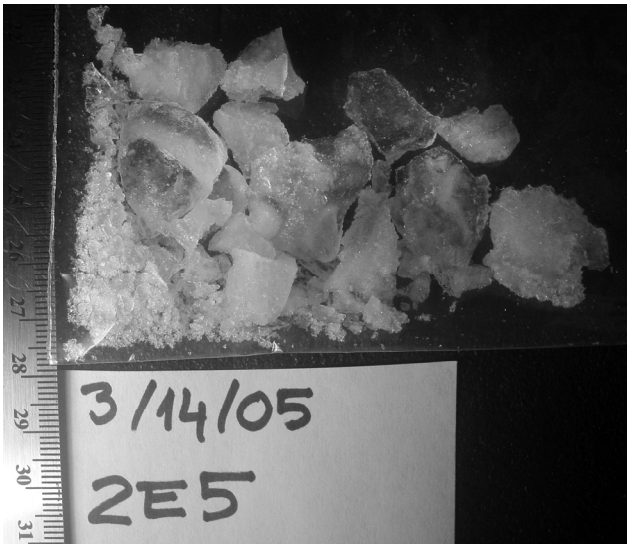

a)

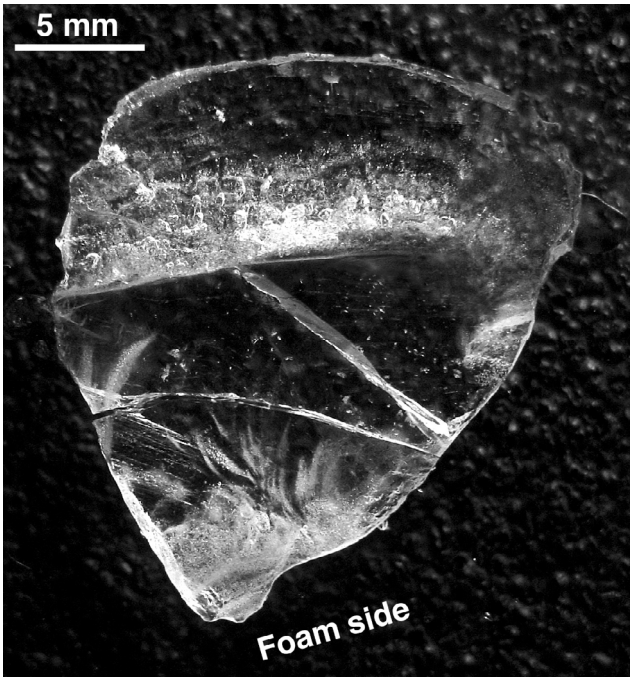

b)

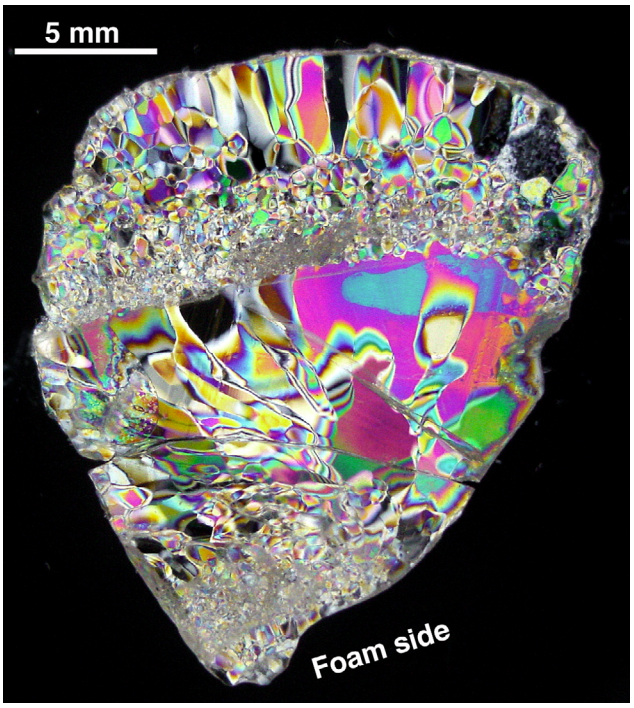

c)

Figure 34: Ice-21, specimen 2E5-3-14/05:
a) macroscopic view;
b) microstructure, direct light;
c) microstructure, polarized.

a)

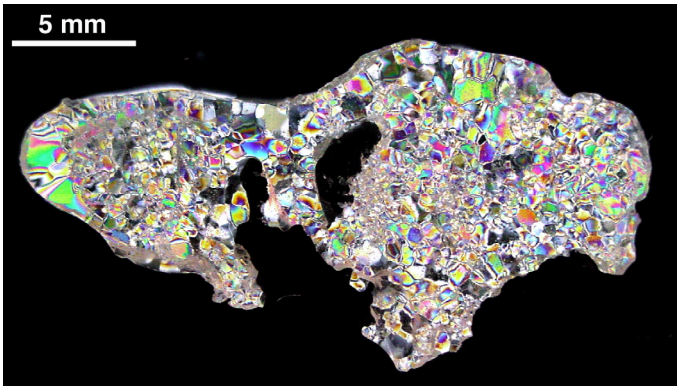

b)

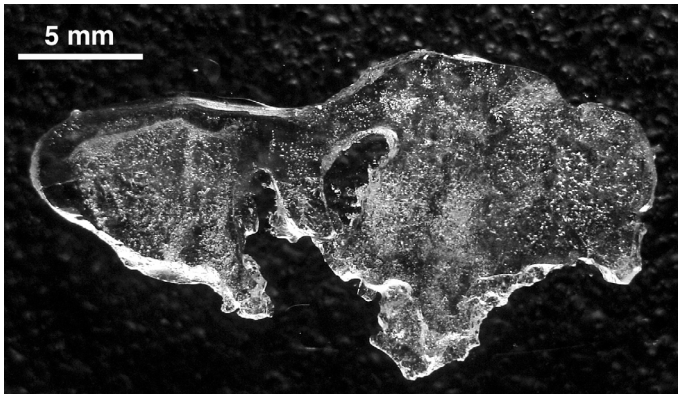

c)

Figure 35: Ice-21, specimen 2BSTRA1-3/14/05:
a) macroscopic view;
b) microstructure, direct light;
c) microstructure, polarized.

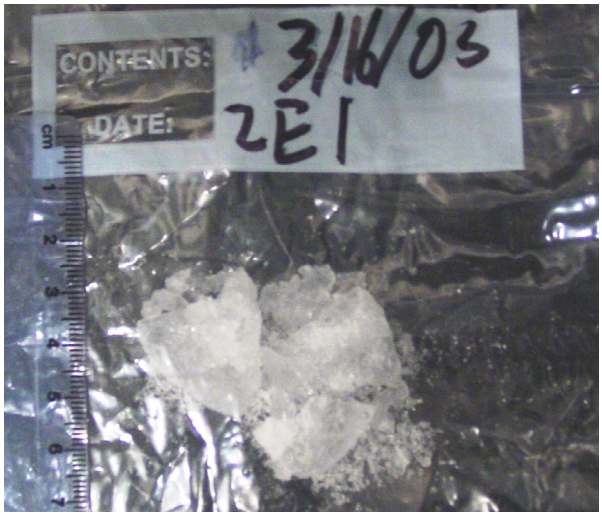

a)

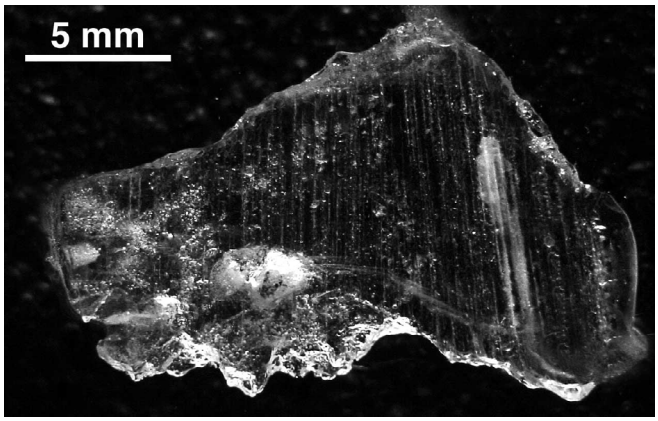

b)

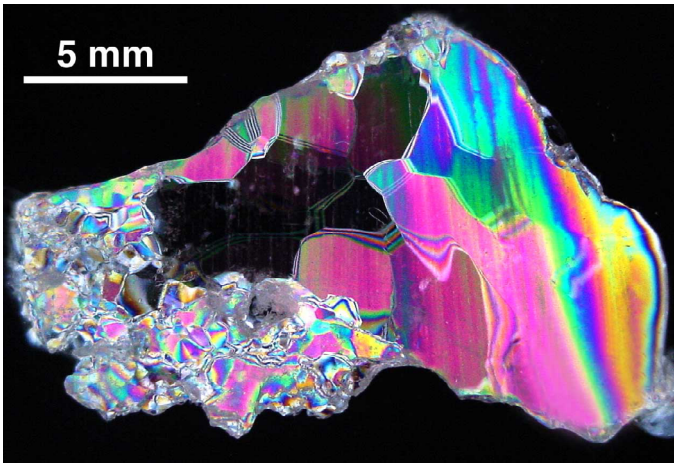

c)

Figure 36: Ice-22, specimen 2E1-3/16/05:
a) macroscopic view;
b) microstructure, direct light;
c) microstructure, polarized.

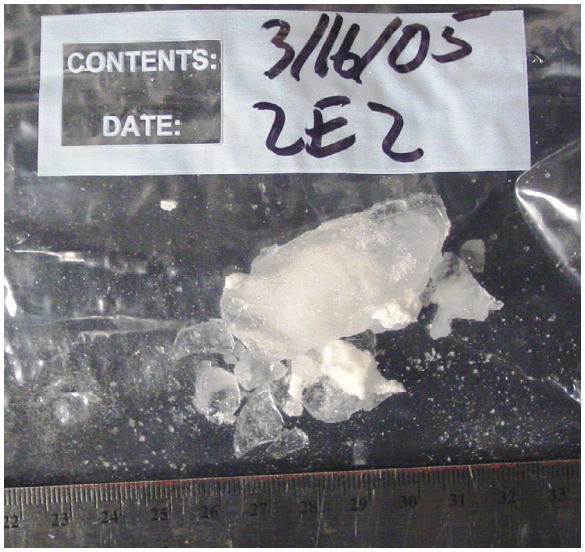

a)

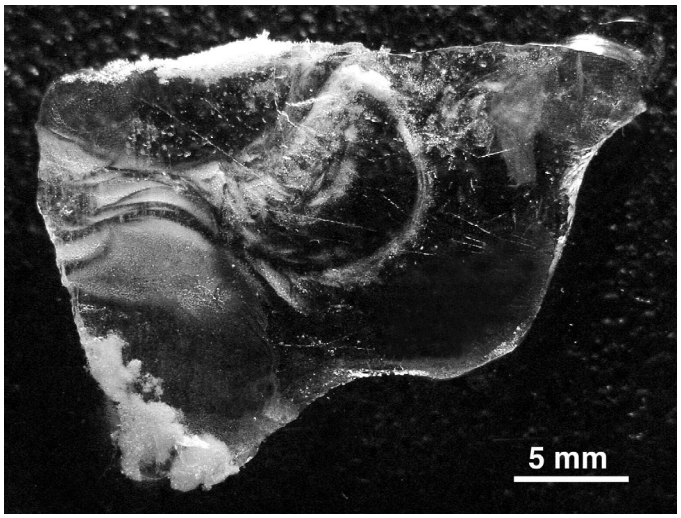

b)

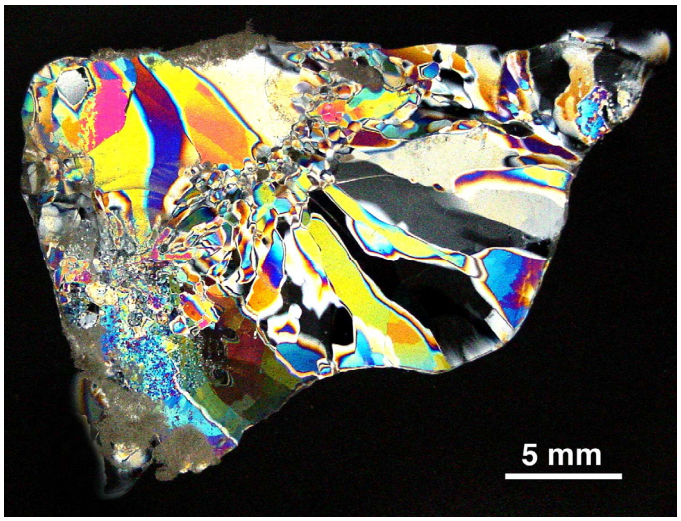

c)

Figure 37: Ice-22, specimen 2E2-3/16/05:
a) macroscopic view;
b) microstructure, direct light;
c) microstructure, polarized.

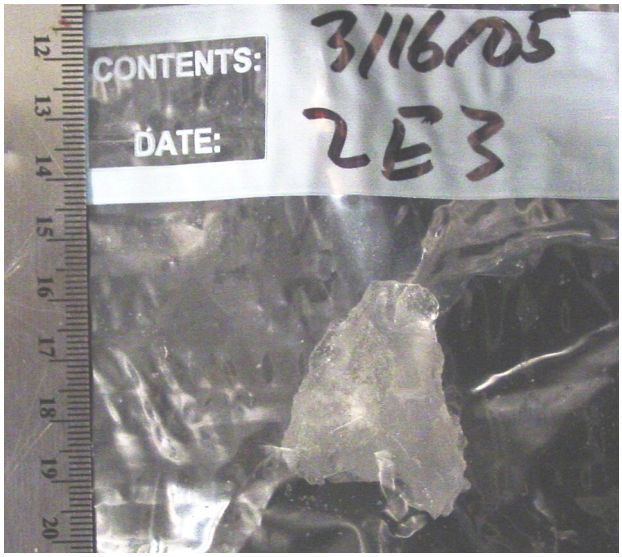

a)

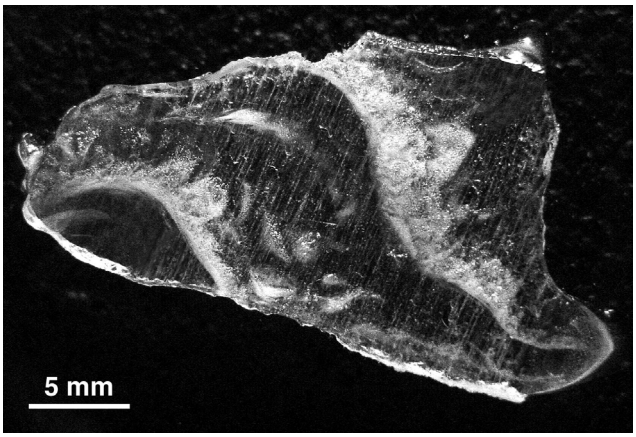

b)

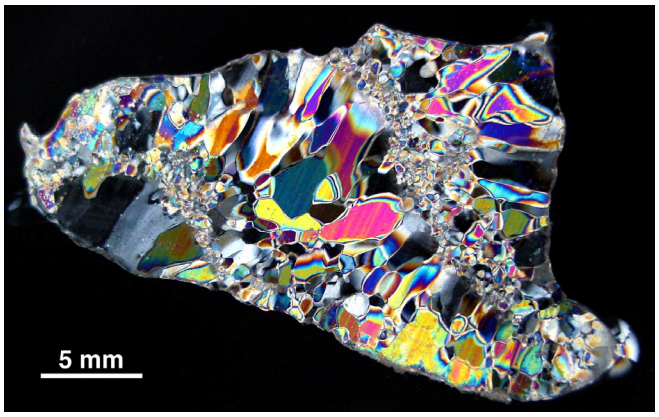

c)

Figure 38: Ice-22, specimen 2E3-3/16/05:
a) macroscopic view;
b) microstructure, direct light;
c) microstructure, polarized.

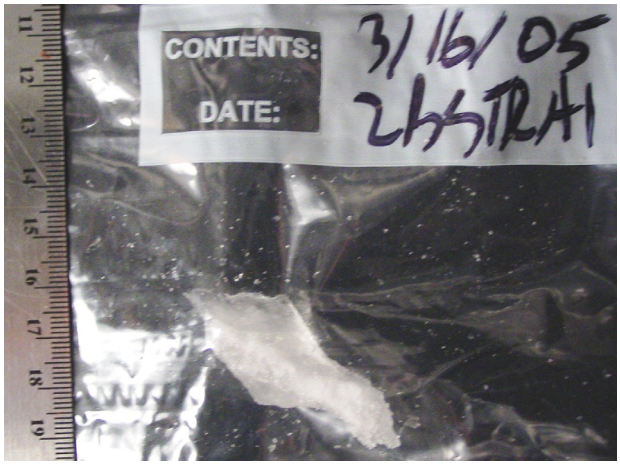

a)

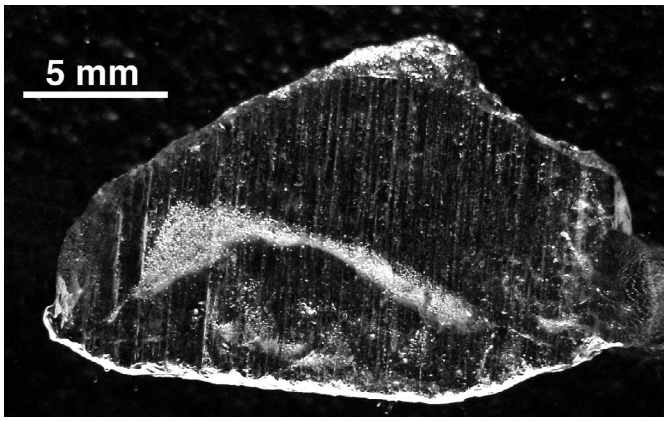

b)

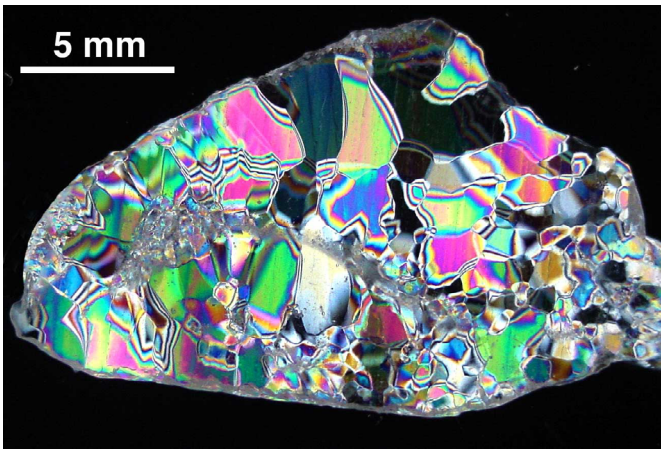

c)

Figure 39: Ice-22, specimen 2BSTRA1-3/16/05:
a) macroscopic view;
b) microstructure, direct light;
c) microstructure, polarized.

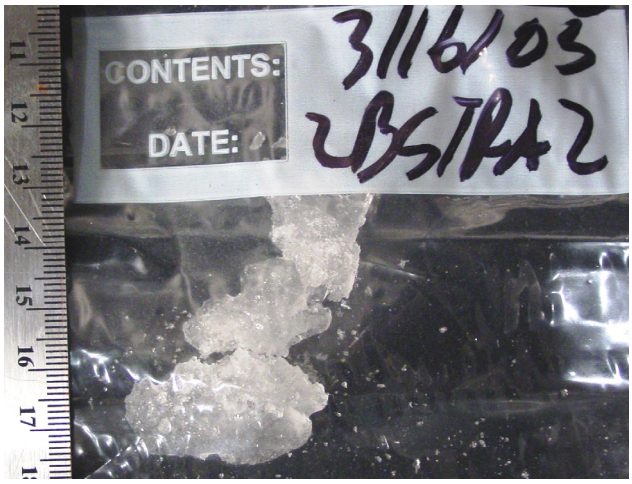

a)

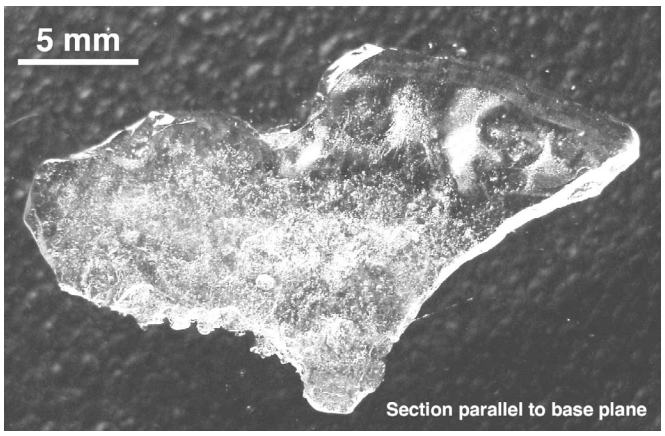

b)

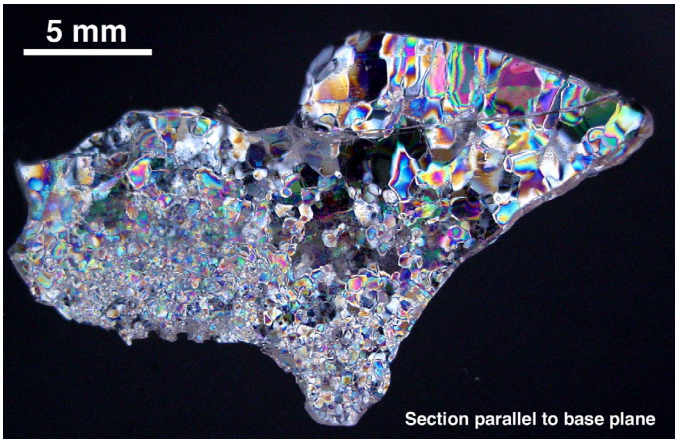

c)

Figure 40: Ice-22, specimen 2BSTRA2-3/16/05:
a) macroscopic view;
b) microstructure, direct light;
c) microstructure, polarized.

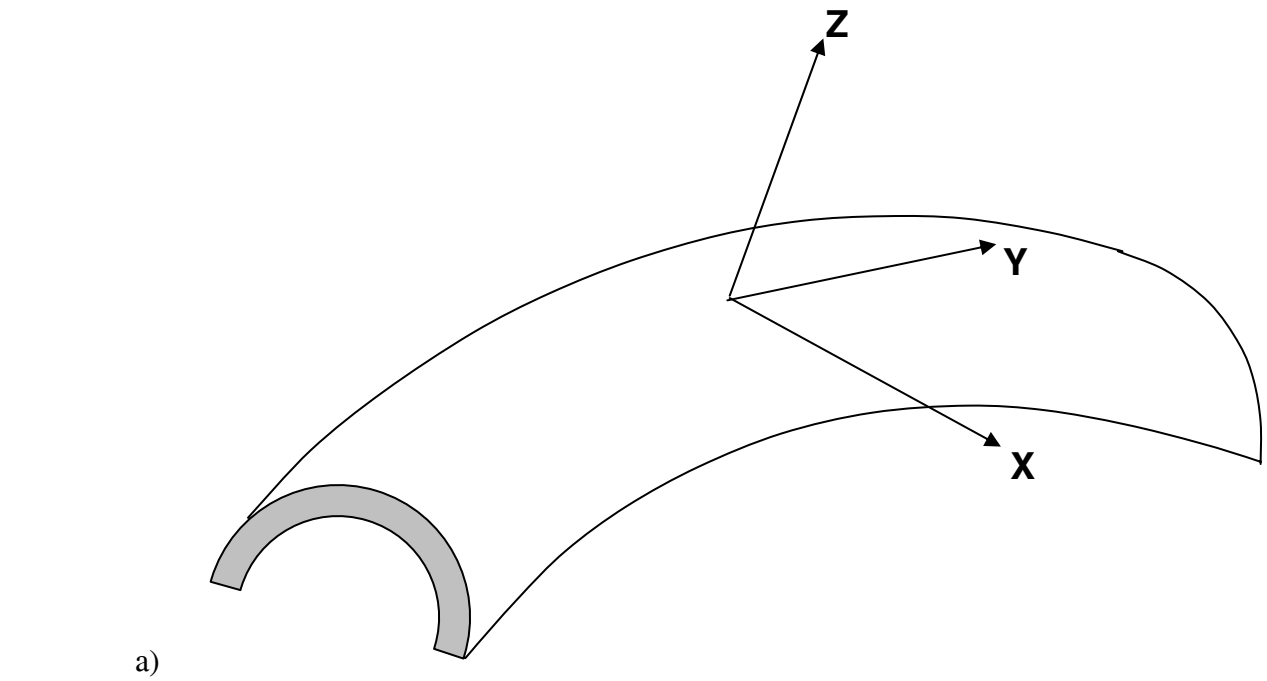

a)

b)

c)

Figure 41: Ice 25:
a) sketch of reference coordinate system for curved beam;
b) photograph of a curved and a straight beam as viewed along direction-Z of a);
c) photograph of a curved and a straight beam as viewed along direction-X of a),

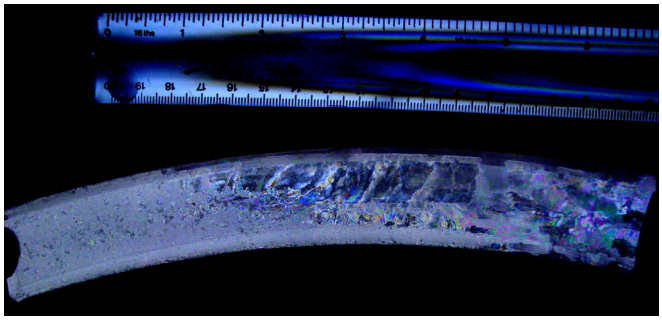

a)

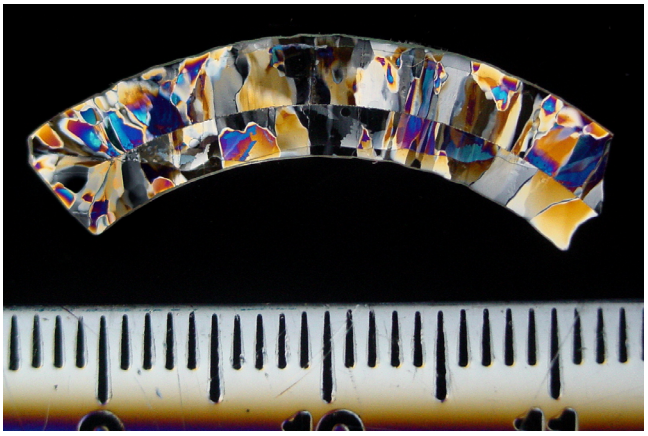

b)

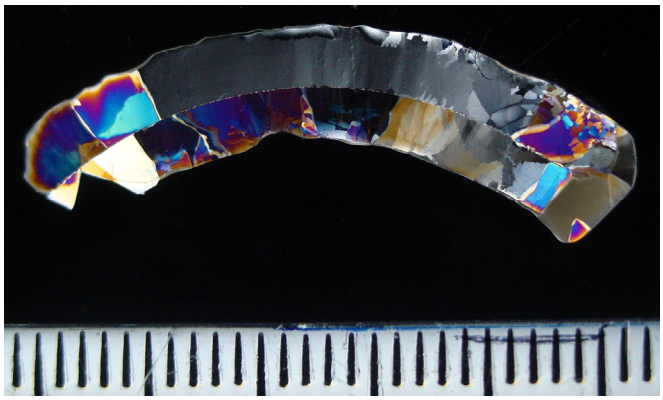

c)

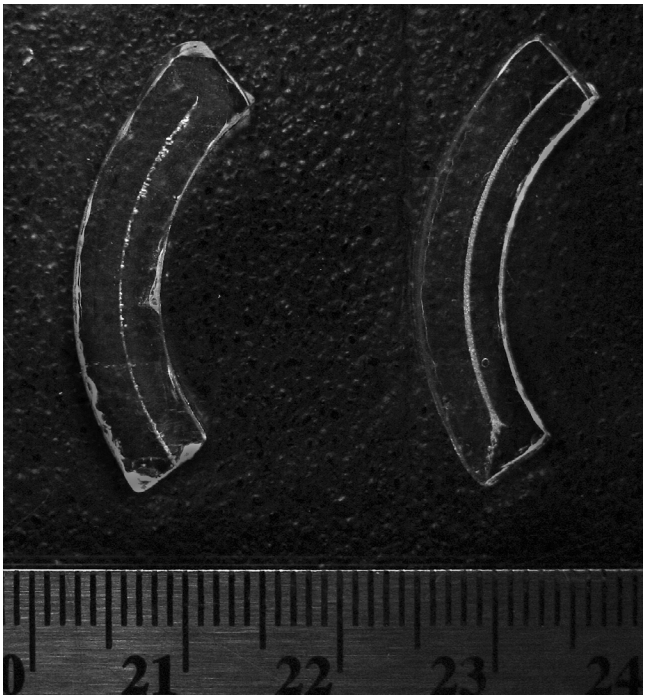

d)

Figure 42: Ice-25, curved beam:
a) overall view as seen along Z-direction;
b) microstructure in XZ section;
c) microstructure in another XZ section;
d) thin-section XZ in direct light showing centerline of bubbles;
e) microstructure in YZ section;
f) as e) in direct light showing centerline of bubbles.

Figure 42 (continued)

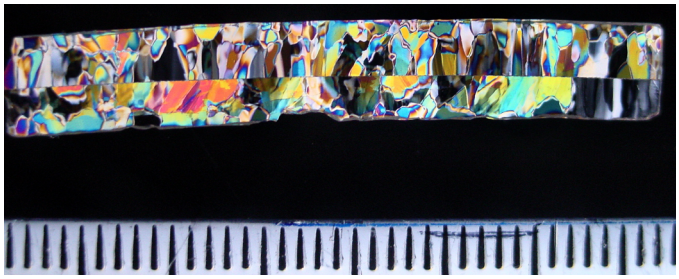

e)

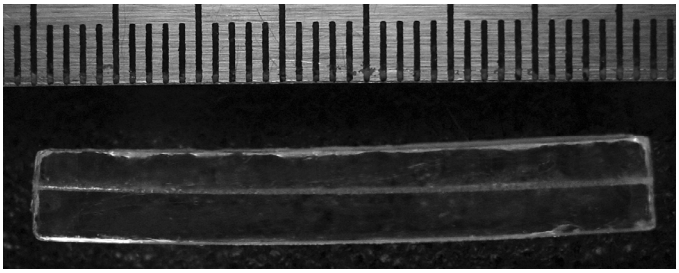

f)

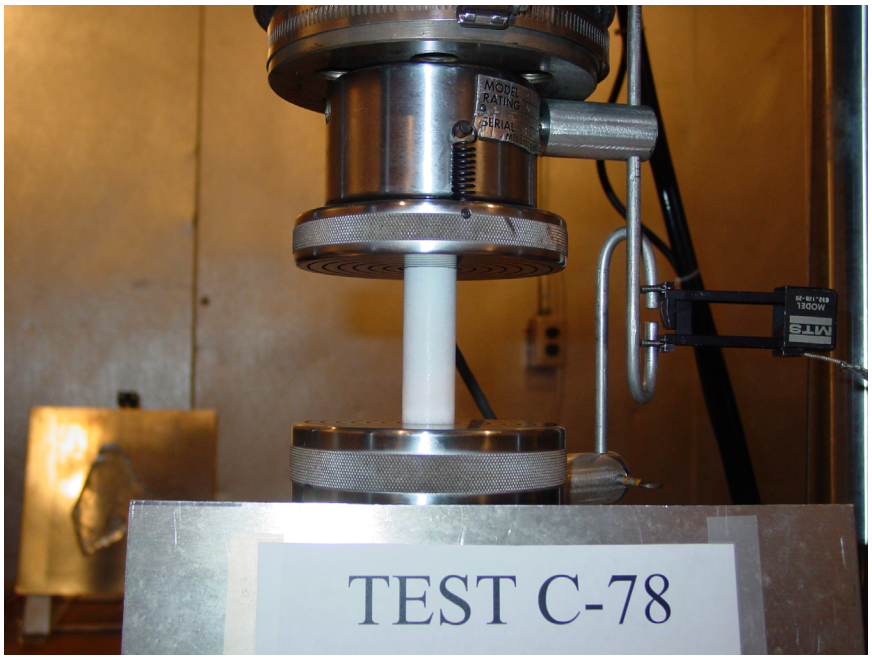

a)

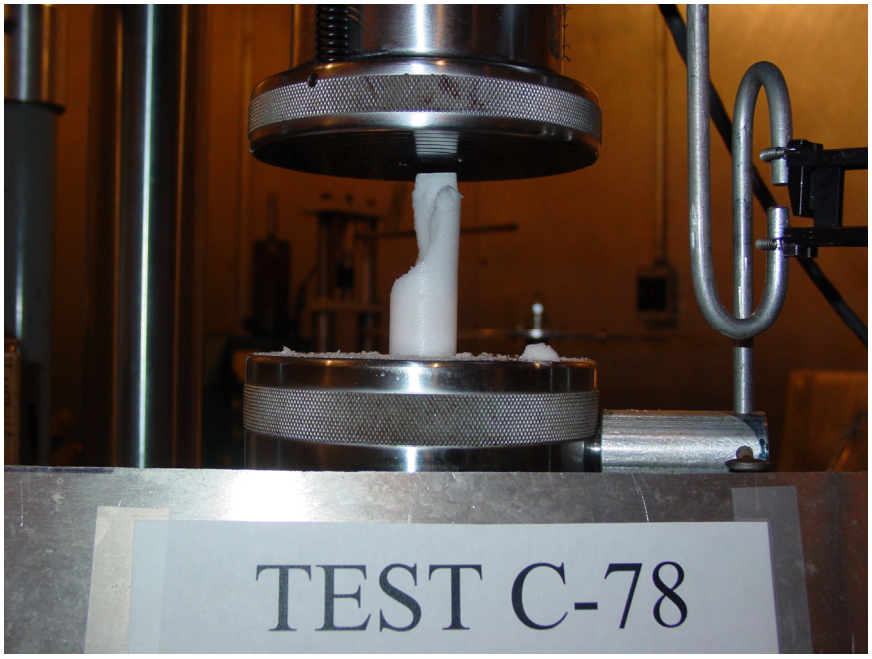

b)

Figure: 43: Photograph showing snow ice in MTS loading system:
a) before loading;
b) after terminal failure.

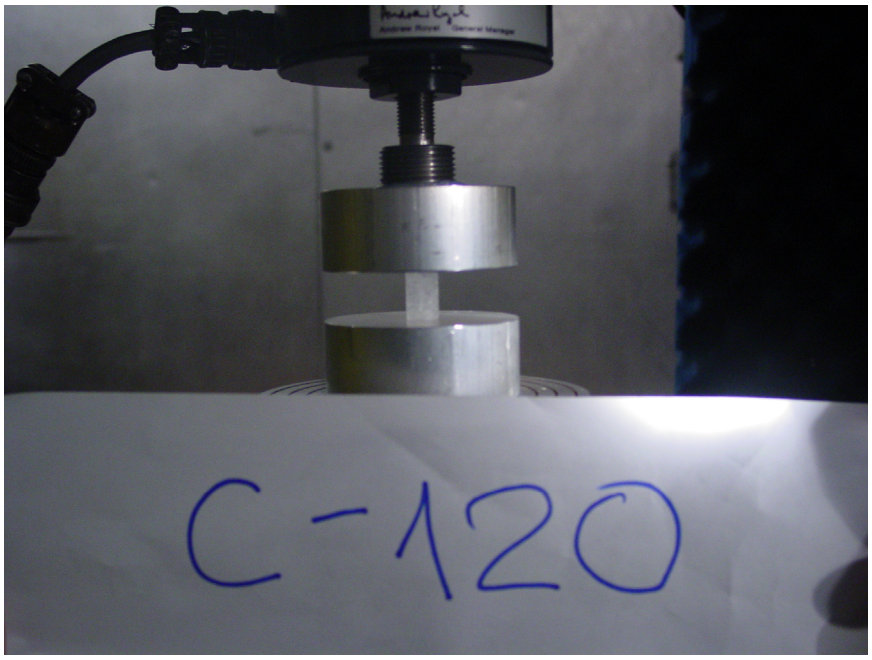

a)

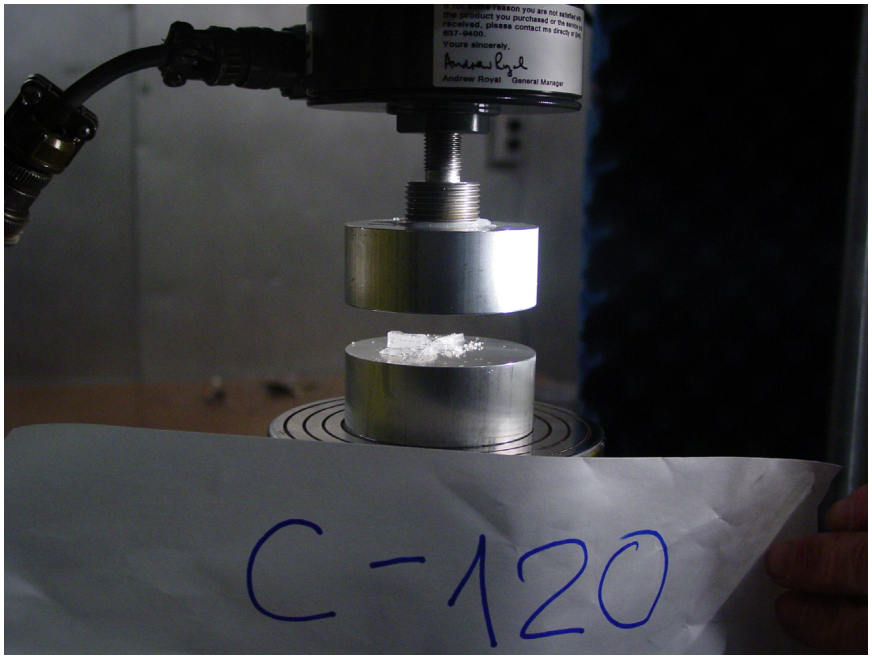

b)

Figure 44: Photograph showing atmospheric ice in MTS loading system:
a) before loading;
b) after terminal failure.

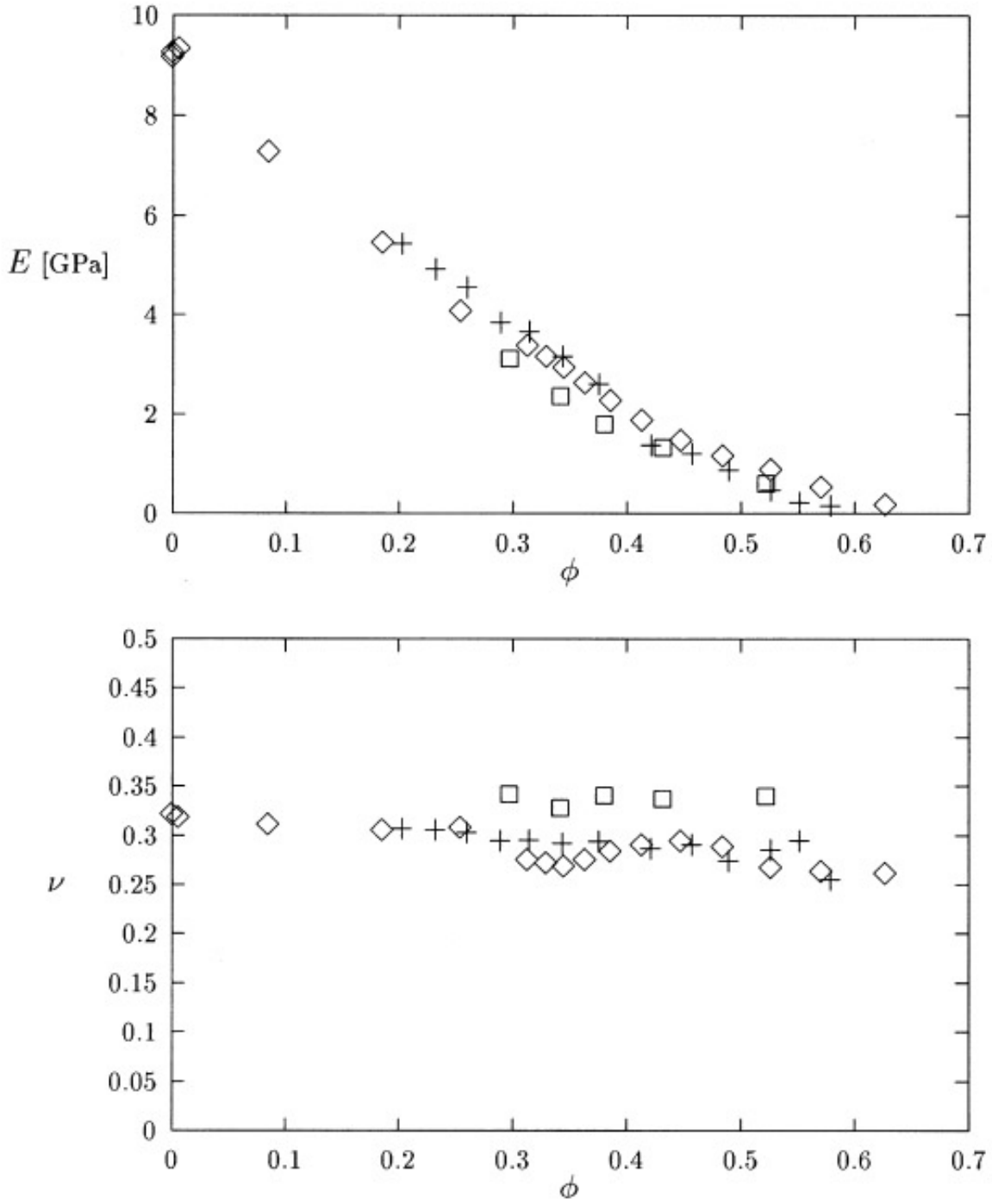

Figure 45: Graphs of Young's modulus, E, and Poisson's ratio, ν, of porous ice versus degree of porosity, ϕ (from Keller et al. 1999).

REPORT DOCUMENTATION PAGE

Form Approved
OMB No. 0704-0188

1. AGENCY USE ONLY (*Leave blank*)	2. REPORT DATE	3. REPORT TYPE AND DATES COVERED
	October 2005	Final Contractor Report

4. TITLE AND SUBTITLE

Characterization of Ice for Return-to-Flight of the Space Shuttle
Part 2—Soft Ice

5. FUNDING NUMBERS

WBS–22–376–10–30–04
NNC05VA04P

6. AUTHOR(S)

Erland M. Schulson and Daniel Iliescu

7. PERFORMING ORGANIZATION NAME(S) AND ADDRESS(ES)

Dartmouth College
Thayer School of Engineering
Hanover, New Hampshire 03755

8. PERFORMING ORGANIZATION REPORT NUMBER

E–15131–2

9. SPONSORING/MONITORING AGENCY NAME(S) AND ADDRESS(ES)

National Aeronautics and Space Administration
Washington, DC 20546–0001

10. SPONSORING/MONITORING AGENCY REPORT NUMBER

NASA CR—2005–213643-PART2

11. SUPPLEMENTARY NOTES

Project Manager, Bradley A. Lerch, Materials and Structures Division, NASA Glenn Research Center, organization code RXL, 216–433–5522.

12a. DISTRIBUTION/AVAILABILITY STATEMENT

Unclassified - Unlimited
Subject Category: 27

Available electronically at http://gltrs.grc.nasa.gov

This publication is available from the NASA Center for AeroSpace Information, 301–621–0390.

12b. DISTRIBUTION CODE

13. ABSTRACT ***(Maximum 200 words)***

In support of characterizing ice debris for return-to-flight (RTF) of NASA's space shuttle, we have determined the microstructure, density and compressive strength (at –10 °C at ~0.3 s^{-1}) of porous or "soft" ice that was produced from both atmospheric water and consolidated snow. The study showed that the atmospheric material was generally composed of a mixture of very fine (0.1 to 0.3 mm) and coarser (5 to 10 mm) grains, plus air bubbles distributed preferentially within the more finely-grained part of the microstructure. The snow ice was composed of even finer grains (~0.05 mm) and contained more pores. Correspondingly, the snow ice was of lower density than the atmospheric ice and both materials were significantly less dense than hard ice. The atmospheric ice was stronger (~3.8 MPa) than the snow ice (~1.9 MPa), but weaker by a factor of 2 to 5 than pore-free hard ice deformed under the same conditions. Zero Values are given for Young's modulus, compressive strength and Poisson's ratio that can be used for modeling soft ice from the external tank (ET).

14. SUBJECT TERMS

Ice; Compression tests; Microstructure; Space shuttles; Impact damage

15. NUMBER OF PAGES

85

16. PRICE CODE

17. SECURITY CLASSIFICATION OF REPORT	18. SECURITY CLASSIFICATION OF THIS PAGE	19. SECURITY CLASSIFICATION OF ABSTRACT	20. LIMITATION OF ABSTRACT
Unclassified	Unclassified	Unclassified	